THE UNIVERSITY OF OKLAHOMA

GRADUATE COLLEGE

A STUDY OF CONSTITUTIVE RELATIONS FOR POLYCRYSTALLINE ALUMINUM DURING FINITE DYNAMIC PLASTIC DEFORMATION

A DISSERTATION

SUBMITTED TO THE GRADUATE FACULTY

in partial fulfillment of the requirements for the

degree of

DOCTOR OF PHILOSOPHY

BY

CHIUDER HSIAO

Norman, Oklahoma

June, 1984

UMI

A STUDY OF CONSTITUTIVE RELATIONS OF POLYCRYSTALLINE ALUMINUM DURING DYNAMIC PLASTIC DEFORMATION

A DISSERTATION

APPROVED FOR THE SCHOOL OF AEROSPACE, MECHANICAL AND NUCLEAR ENGINEERING

By

Akhtar S. Khan

Luther W. White

Charles W. Bert

A R Mukherjee

Darius M. Egle

ABSTRACT

An experimental study is made of the plastic wave propagation in fully annealed and as received 1100-F aluminum subjected to axisymmetric constant-velocity free flight impact in the range of 200 in/sec (5 m/sec) to 3000 in/sec (76 m/sec).

The direct experimental measurements established the applicability of one-dimensional strain-rate-independent finite-amplitude wave theory. These dynamic strain profiles were used to determine a dynamic response function of the form $\sigma - \sigma_Y = \beta(\epsilon - \epsilon_Y)^a$ to describe the character of plastic wave deformation. The results show that there are distinct differences in the behavior when the strain levels are in between inner and outer yield limits and when strain levels are beyond the outer yield limit.

ACKNOWLEDGMENTS

The author would like to express his deep appreciation to his advisor, Professor Akhtar S. Khan, for his patient guidance and encouragement throughout the present study. Also, he is grateful to Professors Charles W. Bert, Davis M. Egle, Anant R. Kukreti, and Luther W. White for reading the manuscript and for suggesting improvements. Many thanks are also given to Mr. William H. Petre for his expert machining and the specimen preparation. Liwen, his wife, her help, constant encouragement and understanding throughout the author's graduate study, is lovingly acknowledged.

The financial support by the School of Aerospace, Mechanical and Nuclear Engineering, the Energy Resources Institute, and the Oklahoma Mining and Mineral Resources Research Institute is gratefully acknowledged.

TABLE OF CONTENTS

	Page
ABSTRACT	iii
ACKNOWLEDGMENTS	iv
TABLE OF CONTENTS	v
LIST OF FIGURES	vi
LIST OF TABLES	ix
Chapter	
I. INTRODUCTION	1
II. EXPERIMENTAL PROCEDURES	9
III. THEORETICAL ANALYSIS	20
IV. EXPERIMENTAL DATA AND DISCUSSION	24
4.1. Description of the experimental results	24
4.2. Dynamic yield limit	34
4.3. Constancy of wave speeds	35
4.4. Experimentally determined dynamic response function	47
4.5. Bell's empirical parabolic stress-strain law	55
4.6. Quasi-static tests	56
4.7. A comparison of observed experimental maximum strain and predicted values	63
V. SUMMARY AND CONCLUSIONS	70
REFERENCES	73

LIST OF FIGURES

Figure		Page
1.	Experimental test setup	10
2.	The potentiometer circuit and the calibration circuit	18
3.	Experimental strain-time history at indicated distances from the impact face for a projectile velocity of 221 in/sec in fully annealed 1100-F aluminum	25
4.	Averaged experimental strain-time history at indicated distances from the impact face for an average projectile velocity of 1637 in/sec in fully annealed 1100-F aluminum	26
5.	Average experimental strain-time history at indicated distances from the impact face for an average projectile velocity of 1651 in/sec in fully annealed 1100-F aluminum	27
6.	Averaged experimental strain-time history at indicated distances from the impact face for an average projectile velocity of 2862 in/sec in fully annealed 1100-F aluminum	28
7.	Experimental strain-time history at indicated distances from the impact face for a projectile velocity of 702 in/sec in as received 1100-F aluminum	29
8.	Experimental strain-time history at indicated distances from the impact face for a projectile velocity of 653 in/sec in as received 1100-F aluminum	30

LIST OF FIGURES (cont'd)

Figure		Page
9.	Averaged experimental strain-time history at indicated distances from the impact face for an average projectile velocity of 1622 in/sec in as received 1100-F aluminum	31
10.	Averaged experimental strain-time history at indicated distances from the impact face for an average projectile velocity of 2811 in/sec in as received 1100-F aluminum	32
11.	Measured average wave speed vs strain (based on Figure 3)	42
12.	Measured average wave speed vs strain (based on Figures 4 and 5)	43
13.	Measured average wave speed vs strain (based on Figure 6)	44
14.	Measured average wave speed vs strain (based on Figure 9)	45
15.	Measured average wave speed vs strain (based on Figure 10)	46
16.	Log-log plot of post-yield strain vs averaged wave speed (based on Figure 3)	49
17.	Log-log plot of post-yield strain vs averaged wave speed (based on Figure 4)	50
18.	Log-log plot of post-yield strain vs averaged wave speed (based on Figure 5)	51
19.	Log-log plot of post-yield strain vs averaged wave speed (based on Figure 6)	52
20.	Log-log plot of post-yield strain vs averaged wave speed (based on Figure 9)	53
21.	Log-log plot of post-yield strain vs averaged wave speed (based on Figure 10)	54

LIST OF FIGURES (cont'd)

Figure		Page
22.	A comparison of the experimentally determined dynamic response function, Bell's experimental parabola, and quasi-static stress-strain curve for fully annealed 1100-F aluminum	57
23.	A comparison of the experimentally determined dynamic response function (parabolic and cubic), Bell's experimental parabola and quasi-static curve for fully annealed 1100-F aluminum	58
24.	A comparison of the experimentally determined dynamic response cubic function and quasi-static stress-strain curve for as received 1100-F aluminum	59
25.	Post-yield stress squared vs strain for quasi-static uniaxial compression test in fully annealed 1100-F aluminum	61
26.	Post-yield stress squared vs strain for quasi-static uniaxial compression test in fully annealed 1100-F aluminum	62
27.	Post-yield stress cube vs strain for quasi-static uniaxial compression test in as received 1100-F aluminum	64

LIST OF TABLES

Table		Page
1.	Chemical analysis of 1100-F aluminum bar ...	12
2.	Geometrical details of the samples	14
3.	Determination of the response function coefficient, β (based on Figure 3)	36
4.	Determination of the response function coefficient, β (based on Figure 4)	37
5.	Determination of the response function coefficient, β (based on Figure 5)	38
6.	Determination of the response function coefficient, β (based on Figure 6)	39
7.	Determination of the response function coefficient, β (based on Figure 9)	40
8.	Determination of the response function coefficient, β (based on Figure 10)	41
9.	A comparison of observed and predicted maximum strains	69

A STUDY OF CONSTITUTIVE RELATIONS FOR POLYCRYSTALLINE ALUMINUM DURING FINITE DYNAMIC PLASTIC DEFORMATION

CHAPTER I

INTRODUCTION

The interest in the plastic behavior of solids subjected to dynamic loading started in the past century[1,2], but this behavior has been studied more extensively in the past three decades (see Bell[3] and Clifton[4] for reviews of these studies). All of these studies can be grouped into three categories. Firstly, the experimental observations in which the wave propagation effects are ignored completely to obtain stress-strain curves at different strain rates (e.g. see Manjoine and Nadai[5]). These have been followed by the second category of experiments by Kolsky[6] in which wave propagation effects were averaged out in order to obtain the behavior of solids. His experimental technique is presently well known as the Split Hopkinson Bar Experiment. The third

category of experiments is the one where strain and particle velocity or displacement histories are obtained at different locations as the stress waves pass these locations. The first investigator to make an attempt to obtain stress-strain curves from strain profiles of finite amplitude waves was Campbell[7]. However, much success with such measurements was achieved only after the development of the diffraction grating technique by Bell[8], particle velocity measurement technique by Malvern[9], and the interferometric strain gage technique by Sharpe[10]. The plate impact experiments[11,12] may also be included in this category since a velocity history profile is obtained on the back surface of an impacted plate. However, since the dimension of the plate in the direction of propagation of the wave is extremely small, the strain rates in the experiment are much higher than other studies in this category. The investigation of Hsu and Clifton[13] also falls in this category.

The research studies in the first category, in which wave propagation effects are completely ignored, provide questionable results. For example, a close look at the experimental results of Manjoine and Nadai[5] reveals a negative strain rate effect (dynamic stresses lower than quasi-static stresses at

a particular strain) in the first half portion of the stress -strain curve, while there is a positive strain rate effect in the remaining portions of the curve. In the experiments of the second type[14-31], in which wave propagation effects are averaged out, a true representation of the dynamic stress -strain curve is obtained only under certain limiting conditions[32-36]. The study of Bertholf and Karnes[35] showed that in order to get reliable results using the Split Hopkinson Bar Technique, the length-to-diameter ratio of the disc should be 0.3 and both faces should be lubricated to theoretically obtain a coefficient of friction of 0.0 at the interfaces. If either of these two conditions is not satisfied, then the stress-strain curve obtained from the experiment even for strain-rate-insensitive materials is higher than the quasi-static curve which may be interpreted incorrectly as a strain rate effect. Obviously, in several of the earlier studies[32-36], especially in the case of dynamic compression and tension investigations, the limitation on the length of the disc was not fulfilled. Thus, the results obtained from the experiments where lengths of the disc were changed to obtain different strain rates, are questionable. An interesting modification to the 'assumed' one-dimensional compressive stress Split Hopkinson Bar

Technique was the uniaxial-strain Split Hopkinson Bar Technique introduced by Bhushan and Jahsman[31]. This strain condition was achieved by putting an elastic collar on the disc so that the radial displacement was prevented.

The conclusions drawn from the results obtained from the experiments in the second category are mixed in nature. Using the torsion, tension, compression, and uniaxial-strain versions of the Split Hopkinson Bar Technique,investigators have frequently reached contradictory conclusions for the same material. For example, using the torsion version of the apparatus, Duffey et al[18] found that the dynamic stress-strain curve for 1100-0 aluminum at a strain rate of 800 sec^{-1} was approximately 50 percent higher than the curve at 10^{-4} sec^{-1}. Using the same torsion version of the technique, Nicholas[23] obtained dynamic and quasi-static curves for the same material which differed by only 10 percent. Further, in another set of tests, Nicholas[23] changed the strain rate in the middle of the tests from 10^{-4} sec^{-1} to 25 sec^{-1} without observing any appreciable change in the response of the material. Thus, depending on which result can be considered as the true representation of the material, it can be concluded that aluminum 1100-0 is either highly strain rate sensitive or negligibly strain rate dependent. It is also possible that

the results using the torsion Split Hopkinson Bar Technique may be dependent on the geometry of the specimen just as in the case for the compression Split Hopkinson Bar Technique[35]. The same material has been studied extensively by others[22,14, 15]; concluding that the material is highly strain rate sensitive. One may also conclude from the above mentioned experiments that the material is much more strain rate sensitive in tension or compression as compared to torsion, but there is no physical basis for such a difference in strain rate sensitivity. Using experiments of this category, similar discrepancies have been observed also in copper[14,17] and 6061-T6 aluminum[29,30,31].

The experiments of Bhushan and Jahsman[31] using a standard disc specimen in dynamic compression (unconfined) and with a collar on the disc specimen (confined) provide very interesting results. The dynamic and quasi-static axial stress-strain curves for confined disc specimens made of 2024-T351 aluminum, 6061-T651 aluminum and oxygen free copper are almost the same while the same curves for unconfined discs are substantially different. In the light of the Bertholf and Karnes study[35], the faces were properly lubricated and the length-to-diameter ratio of the disc was just right. Even then one may make two

different conclusions about the rate sensitivity of the material, depending on which set of data is assumed to be the true characteristic of the material.

Thus, the experiments in the second category where wave propagation effects are averaged, succeed to an extent in providing the dynamic response functions of the crystalline solids. However, these type of experiments are not as effective in providing an understanding of the wave propagation in materials as well as dependence of material behavior on strain rate. Only experiments where strain or velocity profiles are obtained during wave propagation[10,12,37] provide the opportunity for the first time to understand the mechanics and behavior of the propagation of plastic stress waves.

Thus, from the discussions above, it appears that in order to study the plastic wave propagation, experiments of the third type[10,12,38,39] are much better than the other two types. Unfortunately, due to technical difficulties, most of these experiments with only few exceptions (e.g. Bell[37] and Sharpe[40]) were limited to the study of waves with strain amplitudes of less than three percent (measured from a fully annealed state of the material or from states with

different prior work hardening).

In this study an extensive experimental investigation of plastic wave propagation in 1100-F aluminum has been made in three regions of projectile velocities. Fistly, the projectile velocity that produces low strain amplitudes of propagation of stress waves which are near the yield limit is used. Secondly, the projectile velocity is increased so that strain amplitudes are around two percent. Finally, this velocity is around 3000 in/sec (76 m/sec) producing about five and six percent compressive strain wave in fully annealed and as received 1100-F aluminum, respectively. All the experiments are performed by constant -velocity free flight symmetrical impact of two solid or two tubular specimens.

The objective of this study is to provide a detailed understanding of nonlinear behavior of polycrystalline 1100-F aluminum during propagation of different levels of strain amplitudes for compressive waves, particularly, for the very low and very large strain amplitudes. The main purpose of this study is to check the applicability of the one-dimensional strain-rate-independent finite-amplitude wave

theory and to determine the dynamic response function to describe the character of plastic wave deformation.

CHAPTER II

EXPERIMENTAL PROCEDURES

A schematic drawing of the experimental setup is shown in Figure 1. A projectile is fired from a uniform bore, compressed-nitrogen gas gun and impacts the specimen at rest. The gas gun is capable of firing a 0.99 inch (25 mm) diameter cylinder with a gas pressure of 350 psi. The projectile is accelerated to a constant velocity, when it comes out from the gun barrel prior to impact, by porting the muzzle of the gas gun. At the time of impact, the projectile is still partly in the gun muzzle in order to maintain the alignment between projectile and specimen. The projectile velocity just before impact is measured by an optical device consisting of two light beams which aim at two photodiodes (Model AA MRD 500 7931) spaced at one inch (2.54 cm) apart and perpendicular to the line of flight of the projectile. When the projectile intercepts the first light beam, a change in output voltage level of the

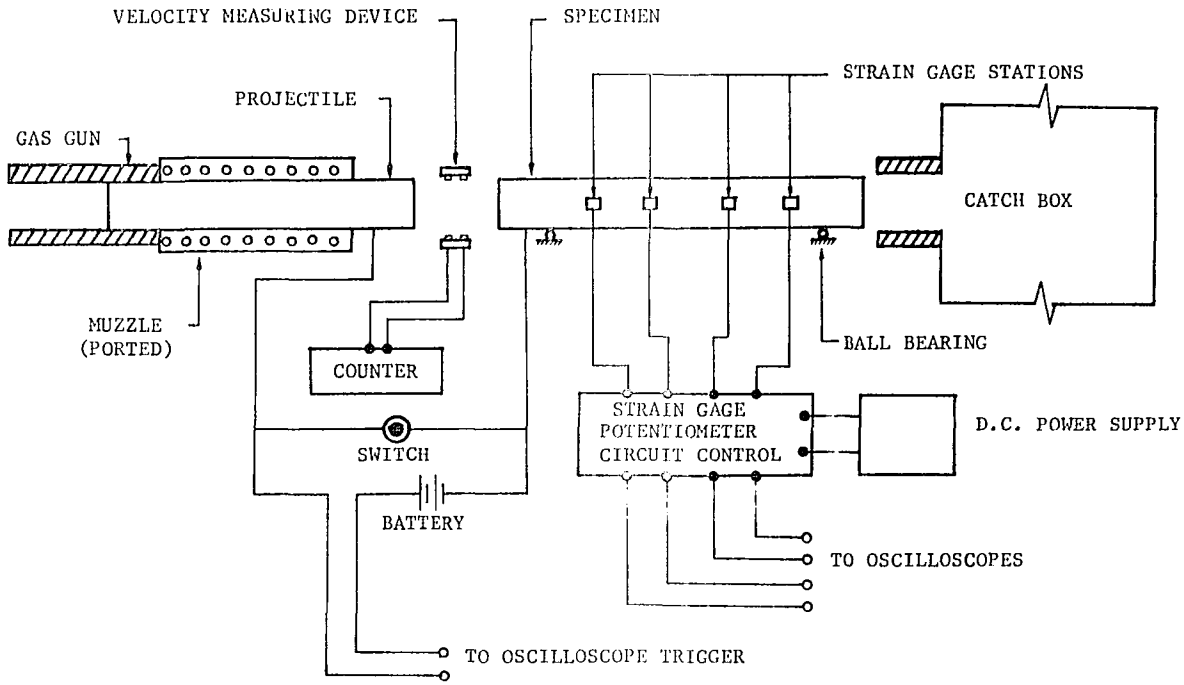

FIGURE 1. EXPERIMENTAL TEST SETUP.

photodiode results which is used as a trigger start signal for an electronic counter (Global Specialties Co. model 5001). Similarly interception of the second light beam results in stopping the counter. Therefore, the time interval of the projectile traveling between the two light beams determines the velocity of the projectile. Simultaneously another method is also employed to measure projectile velocity: the projectile starts and stops a counter when it comes in contact with two wires spaced one inch (2.54 cm) apart. After impact, the projectile and specimen are captured in a catch box.

Two types of samples are used in this experimental study. One is a solid cylinder, while the other is a tubular cylindrical specimen. Every specimen is machined to an outside diameter of 0.989 ± 0.001 inch (25 ± 0.025 mm) from one inch (25.4 mm) diameter 1100-F aluminum bar manufactured by the Aluminum Company of America. A chemical analysis of this alloy of aluminum is given in Table 1. Particular care is taken to make the faces of specimens and projectiles completely flat and perpendicular to their axes. This is done by grinding them with 600-grit silicon-carbide paper on a flat glass plate. After

Table 1

CHEMICAL ANALYSIS OF 1100-F ALUMINUM BAR, WT. %

MILL SOURCE	Mn	Cu	Si+Fe	Zn	Others	Al
ALCOA	0.05 MAX.	0.20 MAX.	1.0 MAX.	1.0 MAX.	0.15 MAX.	97.6 MIN.

these preparations, the precise dimensions of the samples are measured and recorded for each test and are listed in Table 2.

The experimental tests are performed in the 'as received' as well as 'fully annealed' conditions for the axially symmetric free flight impact of two identical samples at room temperature. In the case of fully annealed 1100-F aluminum, the complete annealing is accomplished by raising the temperature to 1100°F (593°C) inside a closed furnace (Lindberg/Hevi-Duty Heating Equipment Co. type 54857-A, capable of operation at temperature to 2200°F) containing the specimen, then keeping it constant for two hours and following this by furnace cooling. Normally, the whole process takes about 24 hours. Bell[3] has pointed out that such an annealing procedure produces a very soft and a fine-grained material and all previous theromo-mechanical history is totally wiped out.

The specimen is instrumented with electric-resistance metallic-foil strain gages at several locations along the length of the specimen. Also, at each location, two gages are mounted on diametrically opposite sides of the specimen

Table 2

GEOMETRICAL DETAILS OF THE SAMPLES

TEST NO.	MATERIAL	DIMENSION OF PROJECTILE				DIMENSION OF SPECIMEN			TYPE OF GAGE USED
	ALUMINUM	OUTSIDE DIAMETER in (mm)	INSIDE DIAMETER in (mm)	LENGTH in (mm)	CAP THICKNESS in (mm)	OUTSIDE DIAMETER in (mm)	INSIDE DIAMETER in (mm)	LENGTH in (mm)	
6	Fully annealed	0.988 (25.10)		10.000 (254.00)		0.988 (25.10)		9.990 (253.8)	KFD-2-C1-11
8	Fully annealed	0.988 (25.10)		10.000 (254.00)		0.988 (25.10)		9.990 (253.8)	TA13-062AH-120
16	Fully annealed	0.988 (25.10)		15.025 (381.64)		0.988 (25.10)		15.025 (381.6)	KFD-1-C1-11
17	Fully annealed	0.988 (25.10)		15.025 (381.64)		0.988 (25.10)		15.025 (381.6)	KFD-1-C1-11
28	As received	0.989 (25.12)	0.739 (18.77)	9.960 (252.98)	0.244 (6.198)	0.989 (25.12)	0.739 (18.77)	10.020 (254.5)	KFE-2-C1
30	As received	0.989 (25.12)	0.739 (18.77)	9.979 (253.47)	0.263 (14.30)	0.989 (25.12)	0.739 (18.77)	10.035 (254.9)	KFD-2-C1-11
32	As received	0.989 (25.12)	0.779 (19.79)	10.135 (257.43)	0.250 (6.350)	0.989 (25.12)	0.779 (19.79)	10.060 (255.5)	KFD-1-C1-11
33	As received	0.989 (25.12)	0.775 (19.69)	10.070 (255.78)	0.244 (6.198)	0.989 (25.12)	0.775 (19.69)	10.070 (255.8)	KFD-1-C1-11

Table 2
(Continued)

TEST NO.	MATERIAL	DIMENSION OF PROJECTILE				DIMENSION OF SPECIMEN			TYPE OF GAGE USED
	ALUMINUM	OUTSIDE DIAMETER in (mm)	INSIDE DIAMETER in (mm)	LENGTH in (mm)	CAP THICKNESS in (mm)	OUTSIDE DIAMETER in (mm)	INSIDE DIAMETER in (mm)	LENGTH in (mm)	
41	As received	0.989 (25.12)	0.773 (19.63)	15.120 (384.05)	0.130 (3.302)	0.989 (25.12)	0.773 (19.63)	15.191 (385.9)	EP-08-015CK-120
43	As received	0.989 (25.12)	0.779 (19.79)	14.955 (379.86)	0.125 (3.175)	0.989 (25.12)	0.779 (19.79)	14.985 (380.6)	EP-08-015CK-120
44	Fully annealed	0.989 (25.12)		10.011 (254.28)		0.989 (25.12)		9.990 (253.8)	KFD-1-C1-11
46	Fully annealed	0.989 (25.12)	0.749 (19.02)	10.04 (255.02)	0.125 (3.175)	0.989 (25.12)	0.749 (19.02)	10.067 (255.7)	EP-08-015CK-120
47	Fully annealed	0.989 (25.12)	0.749 (19.02)	10.00 (254.00)	0.125 (3.175)	0.989 (25.12)	0.749 (19.02)	10.030 (254.8)	EP-08-015CK-120
48	Fully annealed	0.989 (25.12)		10.017 (254.43)		0.989 (25.12)		10.038 (255.0)	KFD-2-C1-11
50	Fully annealed	(Quasi-static test)				0.990 (25.15)		2.000 (50.8)	KFE-5-C1
51	Fully annealed	(Quasi-static test)				0.990 (25.15)		1.500 (38.1)	KFE-5-C1
52	As received	(Quasi-static test)				0.990 (25.15)	0.501 (12.73)	1.010 (25.7)	KFE-5-C1
53	As received	(Quasi-static test)				0.990 (25.15)	0.500 (12.70)	1.030 (26.2)	KFE-5-C1

and connected in series to make the combination insensitive to bending strains. Several types of foil strain gages are used as listed in Table 2. Constantan alloy foil gages with polyimide backing (Precision Foil Technology gage TA13-062AH-120 or Kwoya gage KFD-1-C1-11, KFD-2-C1-11) are normally used for strains less than three percent. Annealed constantan foil gages with polyimide backing (Precision Foil Technology gage PAHE-062CH-120, Kwoya gage KFE-2-C1, KFE-5-C1 or Micro-Measurements gage EP-08-015CK-120) can be used for strains up to eight percent. All gages used for low-amplitude waves (less than three percent) are cemented with the cyanoacrylate Eastman 910 (Micro-Measurements M-Bond 200 Adhesive), while for high elongation, the gages are cemented with the M-Bond AE-15 epoxy system marketed by Micro-Measurements. The gage application techniques recommended by the manufacturer and in a study by Barrowman[41] are followed.

The specimen is supported on an adjustable mechanism with four small ball bearings (TRW Inc. type MRC R3FFM) to provide an unrestricted axial translational motion. The specimen and the projectile are aligned optically, while the projectile is approximate four to five inches in the

gas gun. This is done to insure an axial impact that produces only longitudinal waves in the specimen. The projectile is then pushed in the gun barrel before releasing compressed nitrogen, while the specimen is kept at rest in the same prealigned position.

A potentiometer circuit with a filter and two Tektronix type 5440 and 5441 oscilloscopes with type 5A38, 5A45 plug-in amplifiers measured and displayed the signals of the voltage output from the strain gages as a function of time. These signals are recorded with a Tektronix type C59 oscilloscope camera using Polaroid type 47 film and C-5C oscilloscope camera using Polaroid type 107 film. The signals of the voltage output are converted into equivalent strains using the potentiometer circuit standard equation and gage factor supplied by the manufacturer. The potentiometer circuit is powered by a 30-volt DC power supply (Trans-Tek, Inc. Model D15.100). Before each test, the strain gage circuit is calibrated and photographed by switching a calibration resistance R_c in parallel with the strain gage. Figure 2 shows the potentiometer circuit and calibration circuit. The oscilloscopes are set to trigger due to closing of a circuit when the projectile comes in

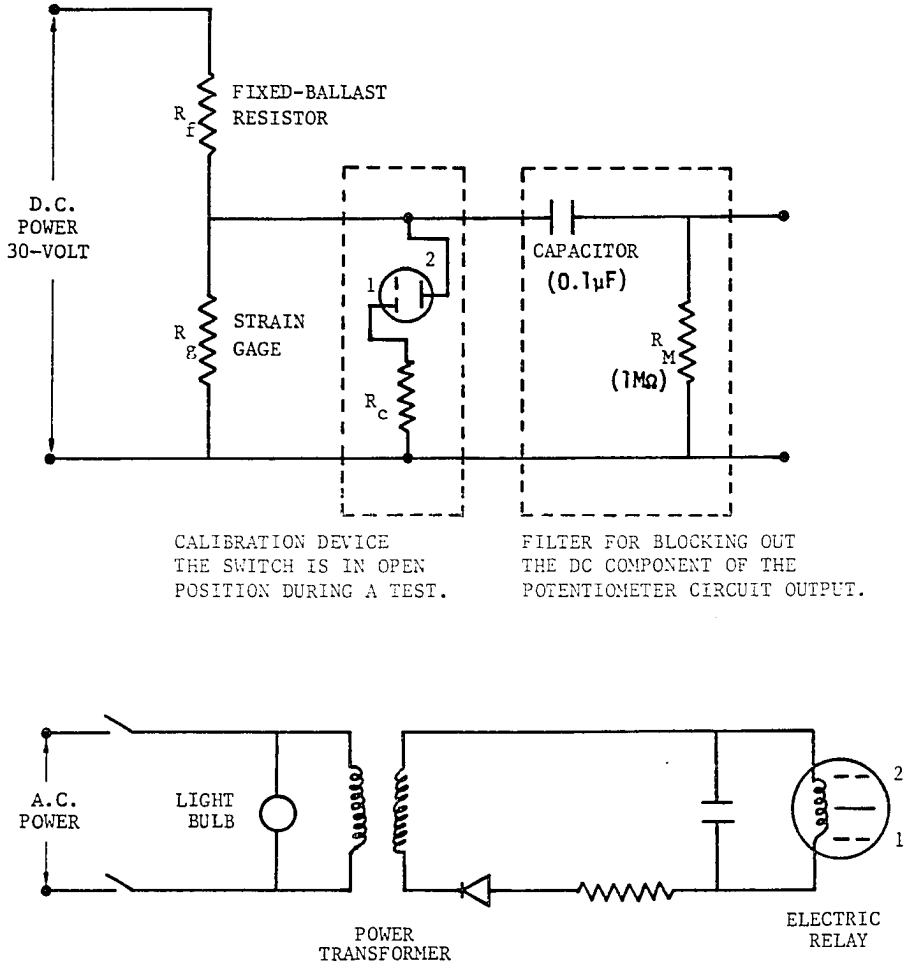

FIGURE 2. THE POTENTIOMETER CIRCUIT (TOP) AND THE CALIBRATION CIRCUIT (BOTTOM).

contact with the specimen as shown in Figure 1.

The quasi-static uniaxial simple compression tests are performed with a standard Riehle testing machine (A Division of AMETEK, Inc. serial no. RA-11417, model FH-60, capacity 60,000 lbs) for comparison with dynamic measurements. These specimens have the same heat treatment as those used in the impact tests. Two flexure-eliminating, high-elongation, 5mm-long foil strain gages are used with their strain outputs recorded by a strain indicator (Micro-Measurements Model P-3500).

CHAPTER III

THEORETICAL ANALYSIS

The discussion of one-dimensional, strain-rate-independent, finite-amplitude wave theory is commonly referred to as the Taylor-Karman theory which was formulated by G.I. Taylor[42] and T. von Karman[43] in 1942. At this same time, similar ideas were independently considered by M.P. White and Le Van Griffis[44].

Let x denote the initial position of a given particle in some homogeneous reference configuration (Lagrangian coordinate) and let ζ denote the present position of the same particle. The present position ζ may be described in terms of the initial position x. Then

$$\zeta = \zeta(x) \tag{1}$$

The axial displacement of the particle is

$$u = \zeta - x \tag{2}$$

Let σ be the nominal or engineering axial stress and ρ the

density of a uniform rod in the undeformed configuration. Then the equation of motion is

$$\frac{\partial^2 u}{\partial t^2} = \frac{1}{\rho}\frac{\partial \sigma}{\partial x} \tag{3}$$

Assuming that nominal stress is a single-valued function of nominal strain for a one-dimensional uniaxial stress wave,

$$\sigma = f(\varepsilon) \tag{4}$$

The dynamic response function f is further assumed to satisfy the conditions:

$$\frac{df}{d\varepsilon} > 0 \quad \text{and} \quad \frac{d^2 f}{d\varepsilon^2} < 0 \tag{5}$$

Introducing eq. (4) into eq. (3), one can express the equation of motion as

$$\frac{\partial^2 u}{\partial t^2} = \frac{1}{\rho}\frac{d\sigma}{d\varepsilon}\frac{\partial \varepsilon}{\partial x}$$

$$= \frac{1}{\rho}\frac{d\sigma}{d\varepsilon}\frac{\partial^2 u}{\partial x^2} \tag{6}$$

where

$$\varepsilon = \frac{\partial u}{\partial x} = \frac{\partial \zeta}{\partial x} - 1 \tag{7}$$

This one-dimensional, finite-amplitude wave equation provides that wave speeds $C_p(\varepsilon)$ should be constant for each level of strain although the value of the constant would differ from one strain amplitude to another, and predicts a relation

between particle velocity v and strain in terms of $C_p(\varepsilon)$. Using the underformed configuration, one finds that these relations have the form prescribed in equations (8) and (9).

$$C_p(\varepsilon) = \left[\frac{1}{\rho}\left(\frac{d\sigma}{d\varepsilon}\right)\right]^{1/2} = \frac{dx}{dt} = \text{constant} \tag{8}$$

$$v = \int_0^{\varepsilon} C_p(\varepsilon)\, d\varepsilon \tag{9}$$

Equation (8) can be examined from experimentally observed strain-time histories for at least three locations comparing wave speeds between locations one and two with those between locations two and three and so on. Similarly equation (9) can be examined by demonstrating the agreement between the observed maximum strains and those obtained from the predicted maximum particle velocity by using eq. (9). If these two conditions of eqs.(8) and (9) are found to hold, then this finite-amplitude strain-rate-independent wave theory is applicable. The desired dynamic response function can be determined experimentally by integrating eq. (8), to obtain

$$\sigma = f(\varepsilon) = \rho \int_0^{\varepsilon} C_p^2(\varepsilon)\, d\varepsilon \tag{10}$$

Using the procedure described above, one can use an alternative approach to interpret the experimental results

within the framework of one-dimensional strain-rate-independent theory. After showing that the wave speeds using strain-time histories of a given level of strain are constant, i.e. eq.(8) holds, then a specific one-dimensional strain-rate-independent general power function will be assumed. Then experimental wave speed data will be used to determine constants in the assumed general power function. After constants have been determined, one has to show that eq.(9) holds by comparing the observed maximum strains with predicted values employing this power function in order to demonstrate that the finite-amplitude strain-rate-independent theory is applicable to nonlinear wave propagation in a particular material.

CHAPTER IV

EXPERIMENTAL DATA AND DISCUSSION

4.1. Description of the experimental results

The experimental results in all of the present tests are obtained under the axially symmetric free flight constant-velocity impact at room temperature. The material, dimension of specimens, and type of strain gage have been described in Table 2. The excellent reproducibility of experimental data at a given projectile velocity is obtained. In Figures 3 to 6, the material used is fully annealed 1100-F aluminum; while from Figures 7 to 10, the material used is as received 1100-F aluminum. In Figure 3 it may be seen the strain-time history at 1,2,3,and 4 inches from the impact face with a low projectile velocity of 221 in/sec. These levels of strain amplitude are slightly above the yield strain of the material. The maximum strain plateau can be observed only at 1 inch (2.54cm) from the impact face before reflected unloading takes place. Figure 4 shows the strain-time history at 1,2,and 3 inches from the impact face. These data obtained from averaging three

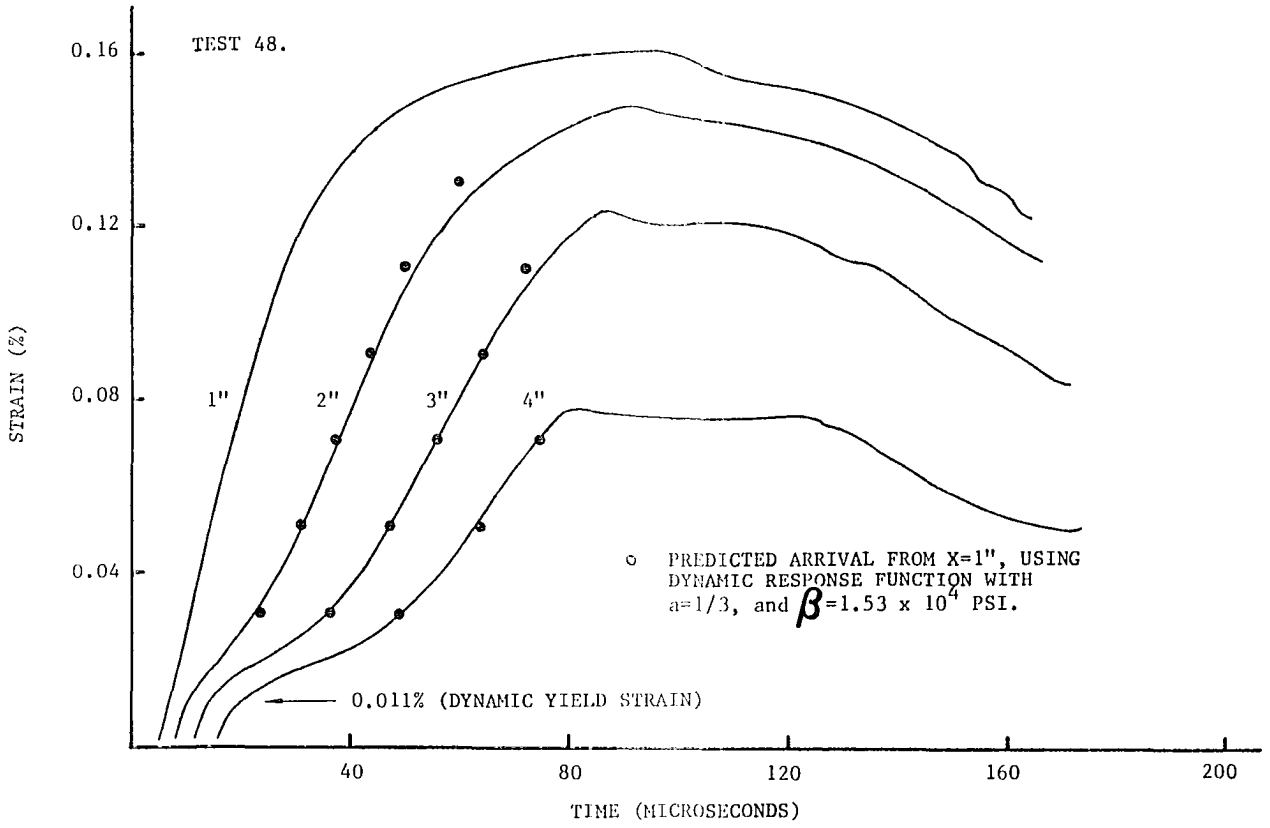

FIGURE 3. EXPERIMENTAL STRAIN-TIME HISTORY AT INDICATED DISTANCES FROM THE IMPACT FACE FOR A PROJECTILE VELOCITY OF 221 IN/SEC IN FULLY ANNEALED 1100-F ALUMINUM.

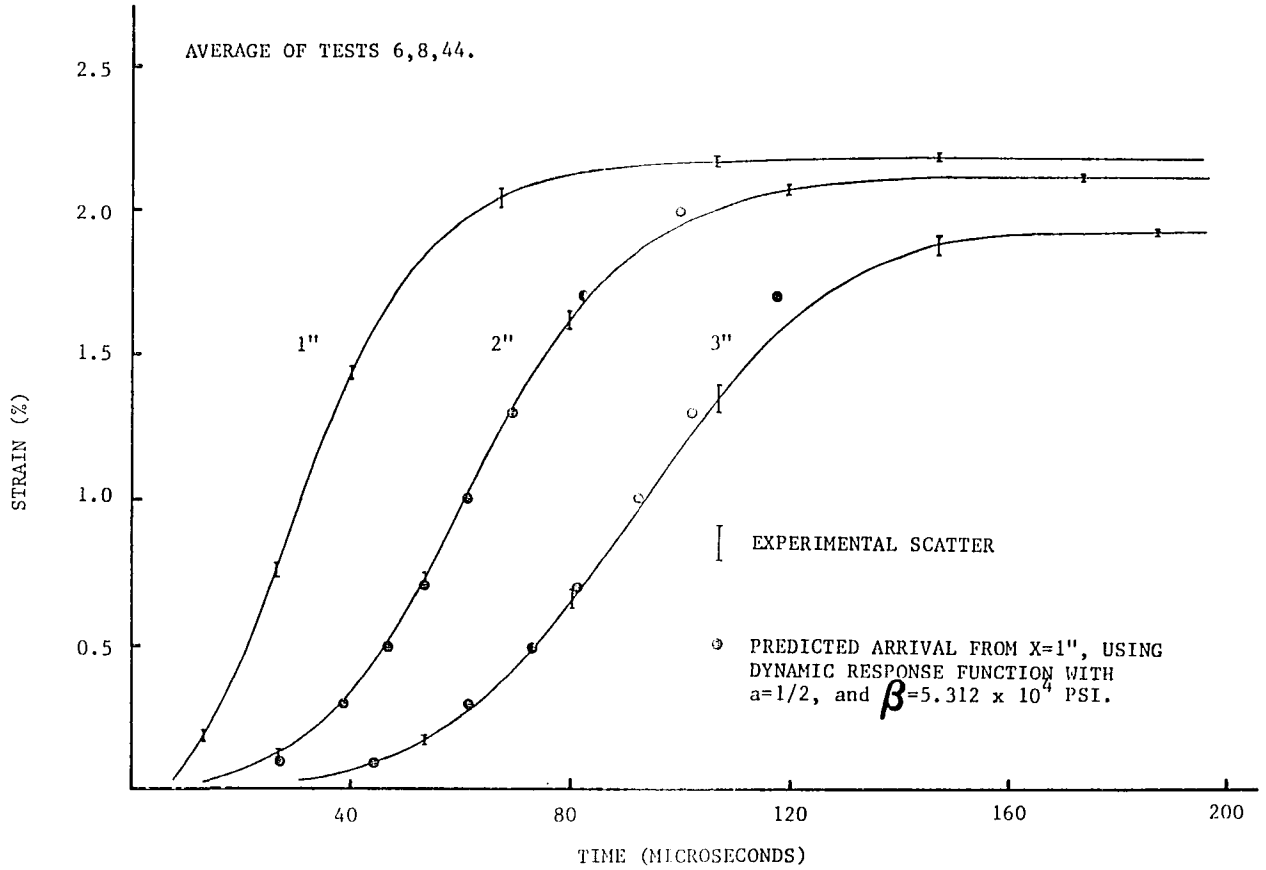

FIGURE 4. AVERAGED EXPERIMENTAL STRAIN-TIME HISTORY AT INDICATED DISTANCES FROM THE IMPACT FACE FOR AN AVERAGE PROJECTILE VELOCITY OF 1637 IN/SEC IN FULLY ANNEALED 1100-F ALUMINUM.

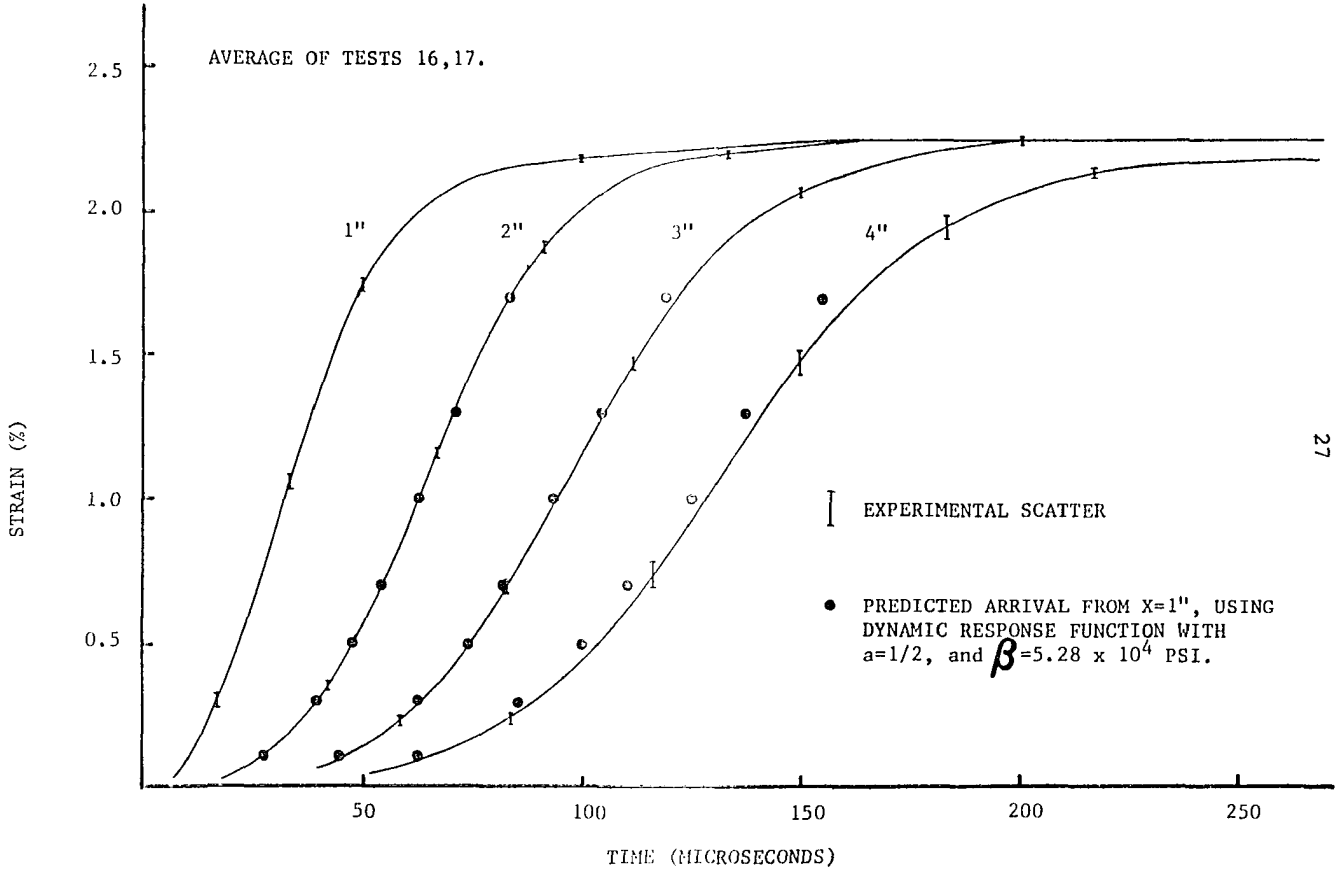

FIGURE 5. AVERAGED EXPERIMENTAL STRAIN-TIME HISTORY AT INDICATED DISTANCES FROM THE IMPACT FACE FOR AN AVERAGE PROJECTILE VELOCITY OF 1651 IN/SEC IN FULLY ANNEALED 1100-F ALUMINUM.

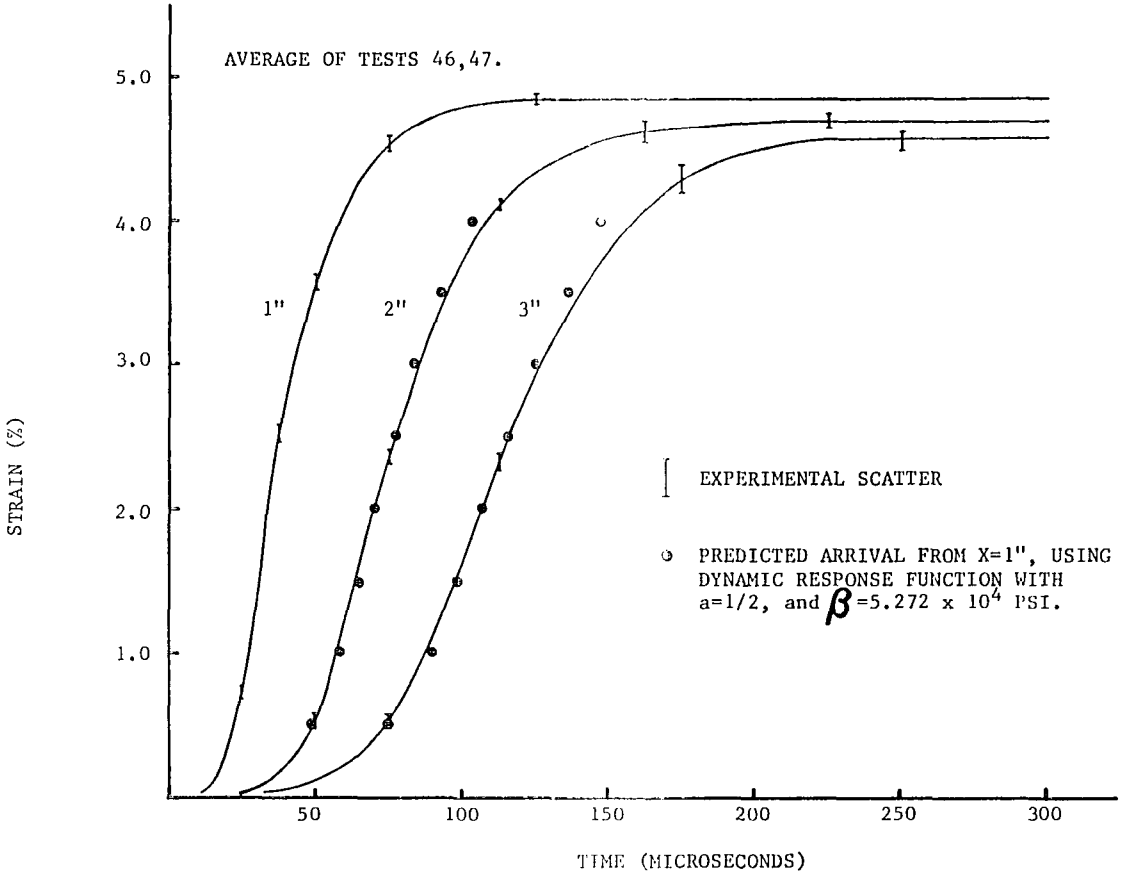

FIGURE 6. AVERAGED EXPERIMENTAL STRAIN-TIME HISTORY AT INDICATED DISTANCES FROM THE IMPACT FACE FOR AN AVERAGE PROJECTILE VELOCITY OF 2862 IN/SEC IN FULLY ANNEALED 1100-F ALUMINUM.

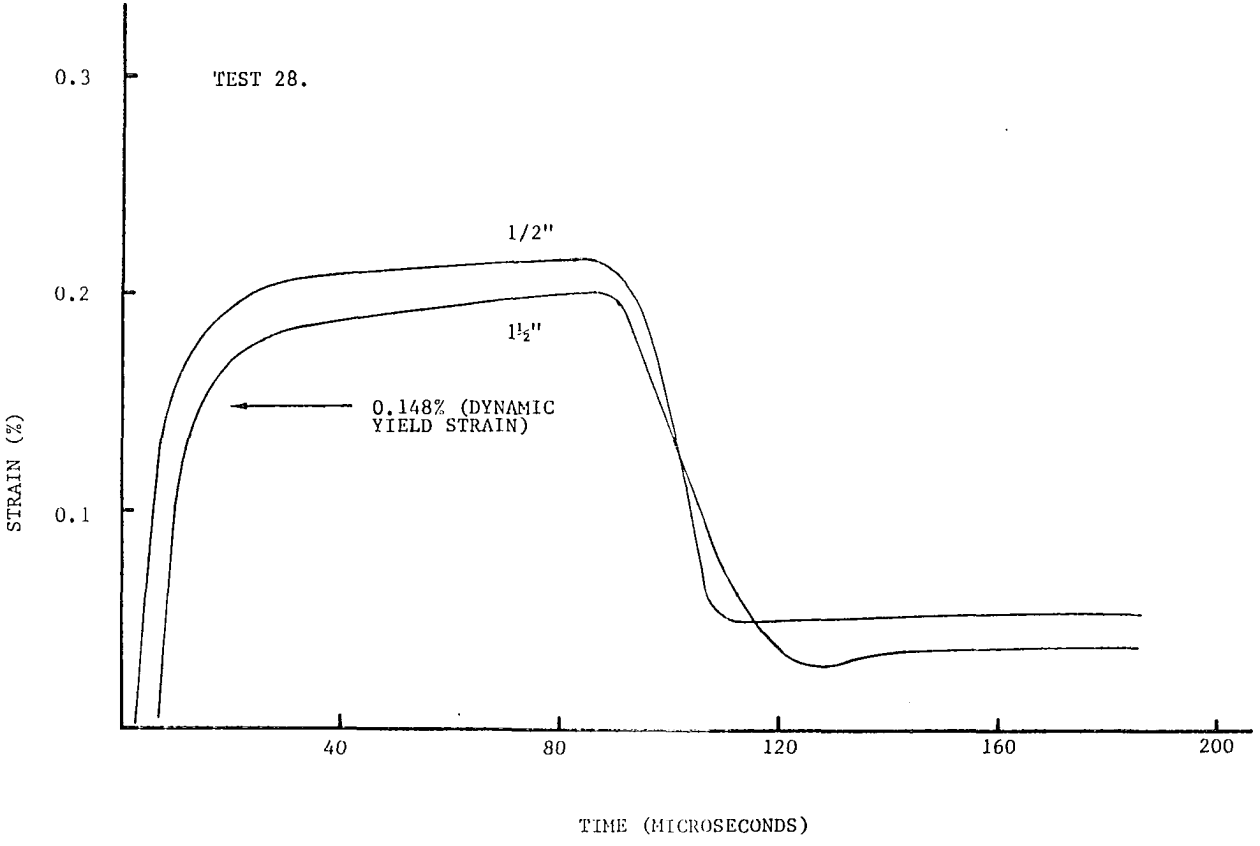

FIGURE 7. EXPERIMENTAL STRAIN-TIME HISTORY AT INDICATED DISTANCES FROM THE IMPACT FACE FOR A PROJECTILE VELOCITY OF 702 IN/SEC IN AS-RECEIVED 1100-F ALUMINUM.

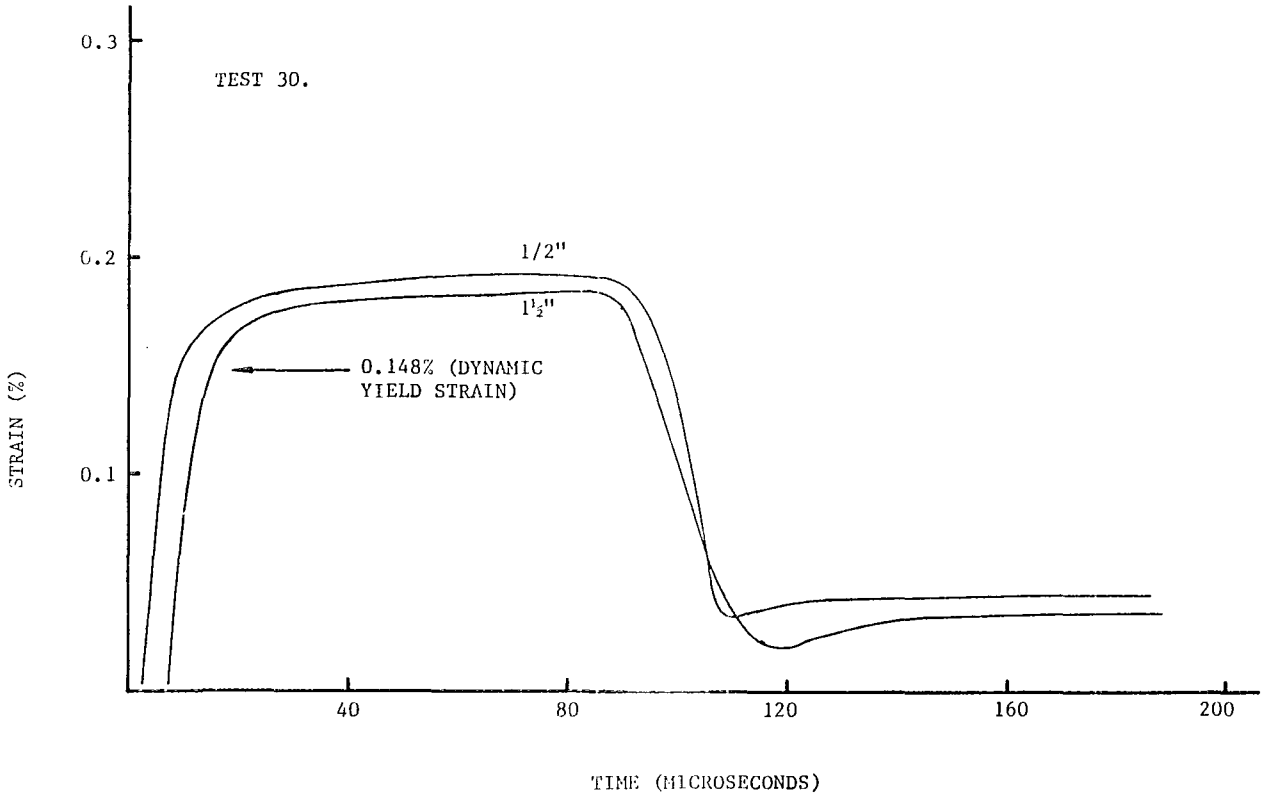

FIGURE 8. EXPERIMENTAL STRAIN-TIME HISTORY AT INDICATED DISTANCES FROM THE IMPACT FACE FOR A PROJECTILE VELOCITY OF 653 IN/SEC IN AS-RECEIVED 1100-F ALUMINUM.

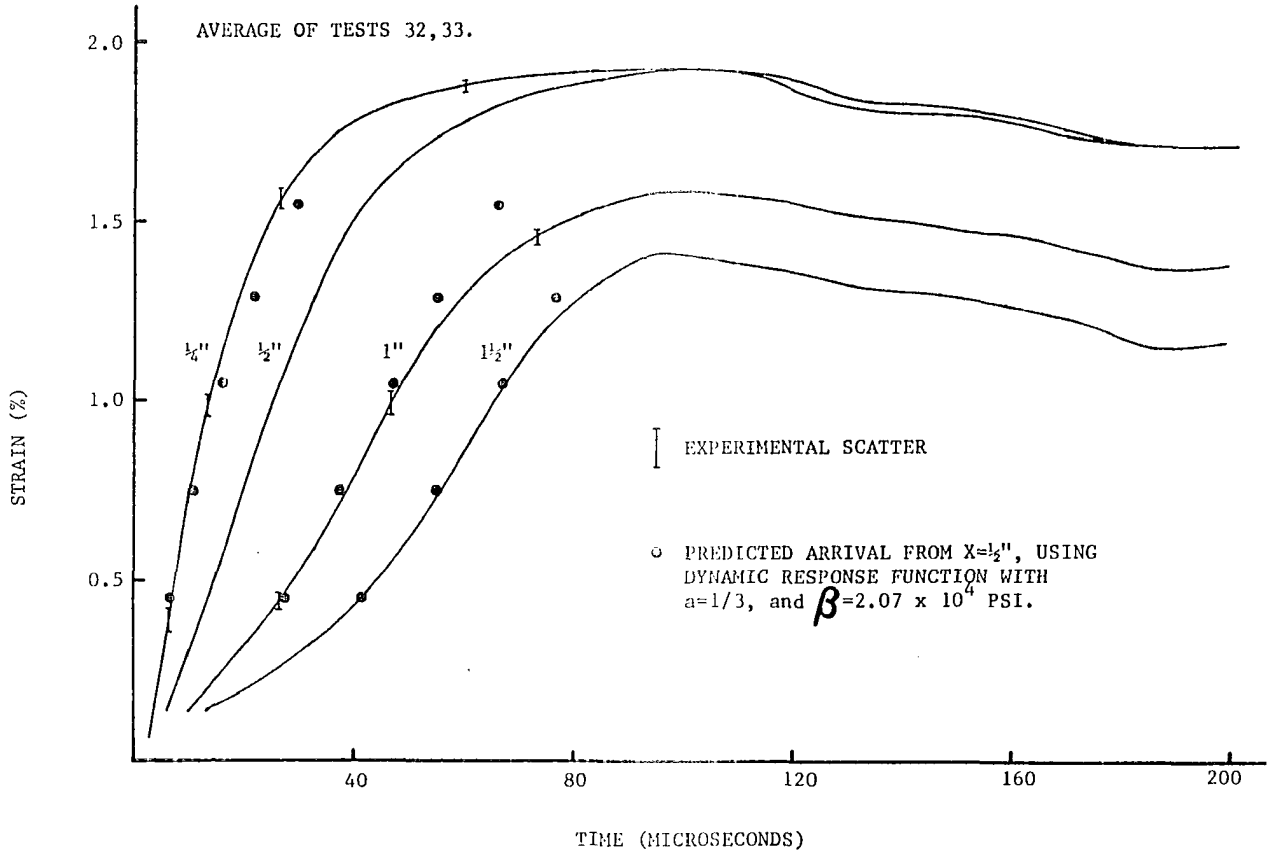

FIGURE 9. AVERAGED EXPERIMENTAL STRAIN-TIME HISTORY AT INDICATED DISTANCES FROM THE IMPACT FACE FOR AN AVERAGE PROJECTILE VELOCITY OF 1622 IN/SEC IN AS-RECEIVED 1100-F ALUMINUM.

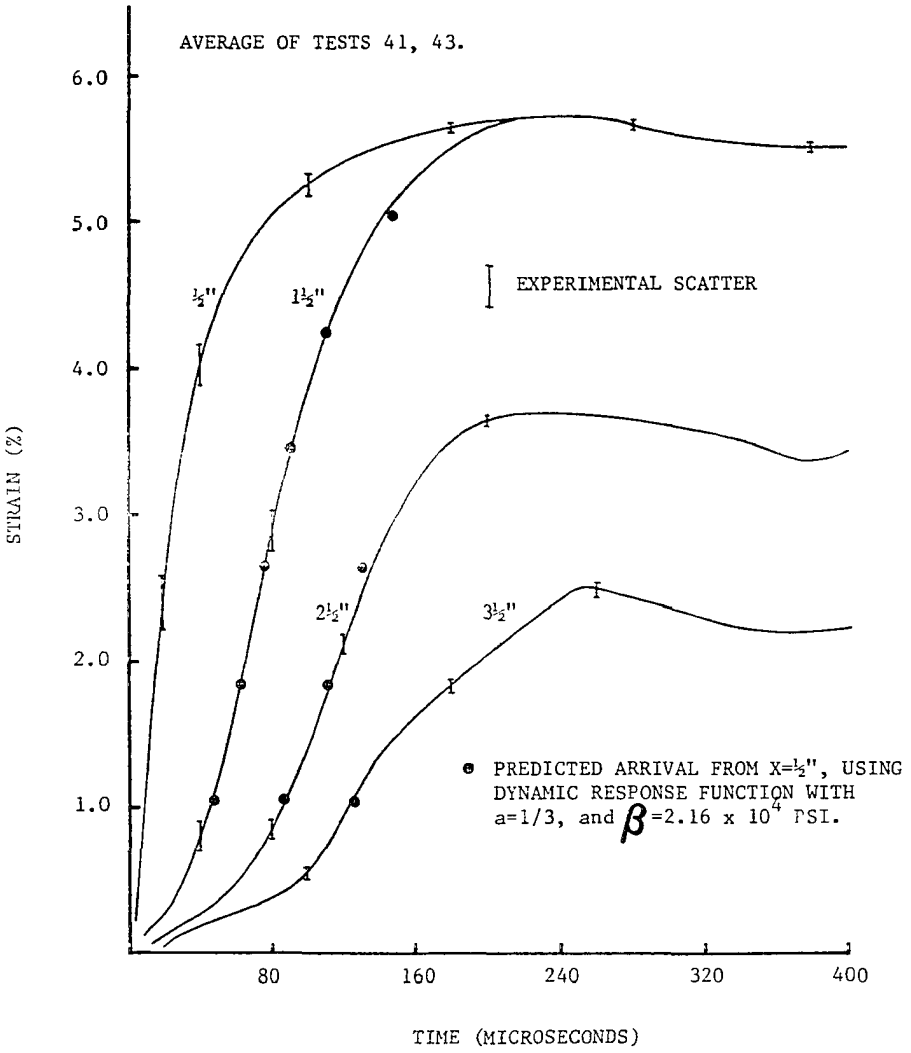

FIGURE 10. AVERAGED EXPERIMENTAL STRAIN-TIME HISTORY AT INDICATED DISTANCES FROM THE IMPACT FACE FOR AN AVERAGE PROJECTILE VELOCITY OF 2811 IN/SEC IN AS-RECEIVED 1100-F ALUMINUM.

tests 6,8,and 44 with projectile velocities of 1656 in/sec, 1621 in/sec and 1634 in/sec, respectively. In this case the strain amplitudes are considerably above the yield strain of the material; thus, the yield strain becomes insignificant as compared to the plastic strain. The constant maximum amplitudes of strain are found to slightly attenuate with distance but this phenomenon occur after the unloading process takes place in a specimen. Therefore tests 16 and 17 are made for extending lengths of specimens under approximately the same conditions used in Figure 4 in order to examine whether the maximum amplitudes of strain remain constant at different locations. Figure 5 gives the strain-time history at 1,2,3,and 4 inches from the impact face. These data obtained from averaging tests 16 and 17 with projectile velocities of 1648 in/sec and 1653 in/sec, respectively. From here, a maximum strain plateau is observed. The average strain-time history at 1,2, and 3 inches from the impact face for the tests 46 and 47 with high projectile velocities of 2873 in/sec and 2851 in/sec, respectively are shown in Figure 6. More large strains up to approximately five percent have been achieved for this high velocity impact. The test 28 of Figure 7 and test 30 of Figure 8 were performed with low projectile

velocities of 702 in/sec and 653 in/sec, respectively such that the strain amplitudes are around and slightly above the yield strain of the material, that is the elastic strains are larger than the plastic strains. In Figure 9 are shown test 32 at 1/4, 1/2, 1, and 1½ inches as well as test 33 at 1/4 and 1 inches from the impact face with projectile velocities of 1627 in/sec and 1616 in/sec, respectively. There is a maximum strain plateau at 1/4 and 1/2 inches. Finally, Figure 10 shows the average strain -time history at 1/2, 1½, 2½, and 3½ inches from the impact face from tests 41 and 43 with projectile velocities of 2815 in/sec and 2807 in/sec, respectively. The maximum strain plateau up to almost six percent is observed at 1/2 and 1½ inches from the impact face.

4.2. Dynamic yield limit

The sudden change in the slope of an observed wave profile for a solid which has a linear elastic domain indicates a yield limit. It is very difficult to determine an accurate yield point from the observed slope change in the strain-time profile employing such a measurement. However, as may be seen in Figures 3,7,and 8, it is possible

to determine approximate values of the dynamic yield strain. For fully annealed 1100-F aluminum, the dynamic yield strain had a value of approximately 0.011%; while for as received 1100-F aluminum, the observed dynamic yield strain was approximately 0.148%. Professor Bell[47] has developed an optical experimental method for accurately measuring the dynamic yield limit from time of contact during axial impact. He determined that the dynamic yield strain in similar specimens to those used in this study, as received 1100-F aluminum, was 0.149%. Also, he determined dynamic yield strain for fully annealed 1100-F aluminum to be 0.0108% by observing strain-time profiles.

4.3. Constancy of wave speeds

By averaging wave speeds between strain gage locations one and two with those between locations two and three and so on from experimental strain-time histories, the constancy of wave speeds can be determined. Such average measured wave speeds are shown in Tables 3 to 8. In Figures 11 to 15 are shown plots of average wave speed as a function of strain. Also shown is the wave speed at which each level of strain is constant.

Table 3

DETERMINATION OF THE RESPONSE FUNCTION COEFFICIENT, β
(BASED ON FIGURE 3)

STRAIN	AVERAGED WAVE SPEED		$\beta = 3\rho c_p^2 (\epsilon - \epsilon_Y)^{2/3}$	
%	10^4 in/sec	(10^2 m/sec)	10^4 psi	(Kg/mm^2)
0.03	7.87	19.99	1.55	10.90
0.04	6.84	17.37	1.56	10.97
0.05	6.12	15.54	1.52	10.69
0.06	5.76	14.63	1.57	11.04
0.07	5.39	13.69	1.55	10.90
0.08	5.16	13.11	1.58	11.11
0.09	4.85	12.32	1.53	10.76
0.10	4.60	11.68	1.49	10.48
0.11	4.24	10.77	1.37	9.63
		AVERAGE β =	1.53	10.72

Table 4

DETERMINATION OF THE RESPONSE FUNCTION COEFFICIENT, β
(BASED ON FIGURE 4)

STRAIN	AVERAGED WAVE SPEED		$\beta = 2\rho c_p^2 (\epsilon - \epsilon_Y)^{1/2}$	
%	10^4 in/sec	(10^2 m/sec)	10^4 psi	(Kg/mm^2)
0.20	4.92	12.50	5.33	37.47
0.30	4.42	11.23	5.32	37.40
0.40	4.10	10.41	5.31	37.33
0.50	3.93	9.98	5.47	38.46
0.60	3.74	9.50	5.43	38.18
0.70	3.64	9.25	5.57	39.16
0.80	3.47	8.81	5.41	38.04
0.90	3.41	8.66	5.55	39.02
1.00	3.28	8.33	5.41	38.04
1.10	3.19	8.10	5.37	37.75
1.20	3.13	7.95	5.41	38.04
1.30	3.05	7.75	5.34	37.54
1.40	2.97	7.54	5.26	36.98
1.50	2.87	7.29	5.09	35.79
1.60	2.77	7.04	4.89	34.38
			AVERAGE β = 5.344	37.57

Table 5

DETERMINATION OF THE RESPONSE FUNCTION COEFFICIENT, β
(BASED ON FIGURE 5)

STRAIN	AVERAGED WAVE SPEED		$\beta = 2\rho c_p^2 (\epsilon - \epsilon_Y)^{1/2}$	
%	10^4 in/sec	(10^2 m/sec)	10^4 psi	(Kg/mm^2)
0.20	4.83	12.27	5.13	36.07
0.30	4.34	11.02	5.13	36.07
0.40	4.09	10.39	5.28	37.12
0.50	3.85	9.78	5.25	36.91
0.60	3.75	9.53	5.46	38.39
0.70	3.58	9.09	5.38	37.83
0.80	3.44	8.74	5.32	37.40
0.90	3.35	8.51	5.35	37.61
1.00	3.23	8.20	5.25	36.91
1.10	3.16	8.03	5.27	37.05
1.20	3.07	7.80	5.20	36.56
1.30	3.05	7.75	5.34	37.54
1.40	2.98	7.57	5.30	37.26
1.50	2.92	7.42	5.26	36.98
1.60	2.86	7.26	5.22	36.70
		AVERAGE β =	5.28	37.12

Table 6

DETERMINATION OF THE RESPONSE FUNCTION COEFFICIENT, β
(BASED ON FIGURE 6)

STRAIN %	AVERAGED WAVE SPEED 10^4 in/sec	(10^2 m/sec)	$\beta = 2\rho c_p^2 (\epsilon - \epsilon_Y)^{1/2}$ 10^4 psi	(Kg/mm^2)
0.30	4.42	11.22	5.32	37.40
0.40	4.12	10.46	5.36	37.68
0.60	3.80	9.65	5.61	39.44
0.80	3.51	8.92	5.54	38.95
1.00	3.34	8.48	5.61	39.44
1.20	3.14	7.98	5.44	38.25
1.40	3.00	7.62	5.37	37.75
1.60	2.91	7.39	5.40	38.00
1.80	2.80	7.11	5.31	37.33
2.00	2.73	6.93	5.32	37.40
2.20	2.66	6.76	5.30	37.26
2.40	2.60	6.60	5.29	37.19
2.60	2.52	6.40	5.17	36.35
2.80	2.44	6.20	5.03	35.36
3.00	2.40	6.10	5.04	35.43
3.20	2.39	6.07	5.16	36.29
3.40	2.37	6.02	5.23	36.77
3.60	2.33	5.92	5.20	36.56
3.80	2.26	5.74	5.03	35.36
4.00	2.22	5.64	4.98	35.01
4.20	2.20	5.59	5.01	35.22
		AVERAGE β =	5.272	37.07

Table 7

DETERMINATION OF THE RESPONSE FUNCTION COEFFICIENT, β
(BASED ON FIGURE 9)

STRAIN	AVERAGED WAVE SPEED		$\beta = 3\rho c_p^2 (\epsilon - \epsilon_Y)^{2/3}$	
%	10^4 in/sec	(10^2 m/sec)	10^4 psi	(Kg/mm^2)
0.30	4.63	11.76	2.15	15.12
0.40	3.89	9.88	2.12	14.91
0.50	3.47	8.81	2.11	14.83
0.60	3.15	8.00	2.06	14.48
0.70	2.98	7.57	2.10	14.76
0.80	2.88	7.32	2.19	15.40
0.90	2.64	6.71	2.03	14.27
1.00	2.58	6.55	2.11	14.83
1.10	2.44	6.20	2.03	14.27
1.20	2.34	5.94	2.00	14.06
1.30	2.18	5.54	1.84	12.94
		AVERAGE β =	2.07	14.53

Table 8

DETERMINATION OF THE RESPONSE FUNCTION COEFFICIENT, β
(BASED ON FIGURE 10)

STRAIN %	AVERAGED WAVE SPEED 10^4 in/sec	(10^2 m/sec)	$\beta = 3\rho c_p^2 (\epsilon - \epsilon_Y)^{2/3}$ 10^4 psi	(Kg/mm^2)
0.50	3.57	9.07	2.23	15.68
0.75	2.94	7.47	2.17	15.26
1.00	2.68	6.81	2.27	15.96
1.25	2.48	6.30	2.31	16.24
1.50	2.28	5.79	2.24	15.75
1.75	2.17	5.51	2.27	15.96
2.00	2.07	5.26	2.27	15.96
2.25	1.92	4.88	2.13	14.98
2.50	1.84	4.67	2.11	14.83
2.75	1.79	4.55	2.13	14.98
3.00	1.72	4.37	2.09	14.69
3.25	1.69	4.29	2.14	15.05
3.50	1.66	4.22	2.17	15.26
3.75	1.61	4.09	2.14	15.05
4.00	1.55	3.94	2.08	14.62
4.25	1.54	3.91	2.14	15.05
4.50	1.50	3.81	2.11	14.83
4.75	1.46	3.71	2.08	14.62
5.00	1.43	3.63	2.06	14.48
		AVERAGE β =	2.16	15.22

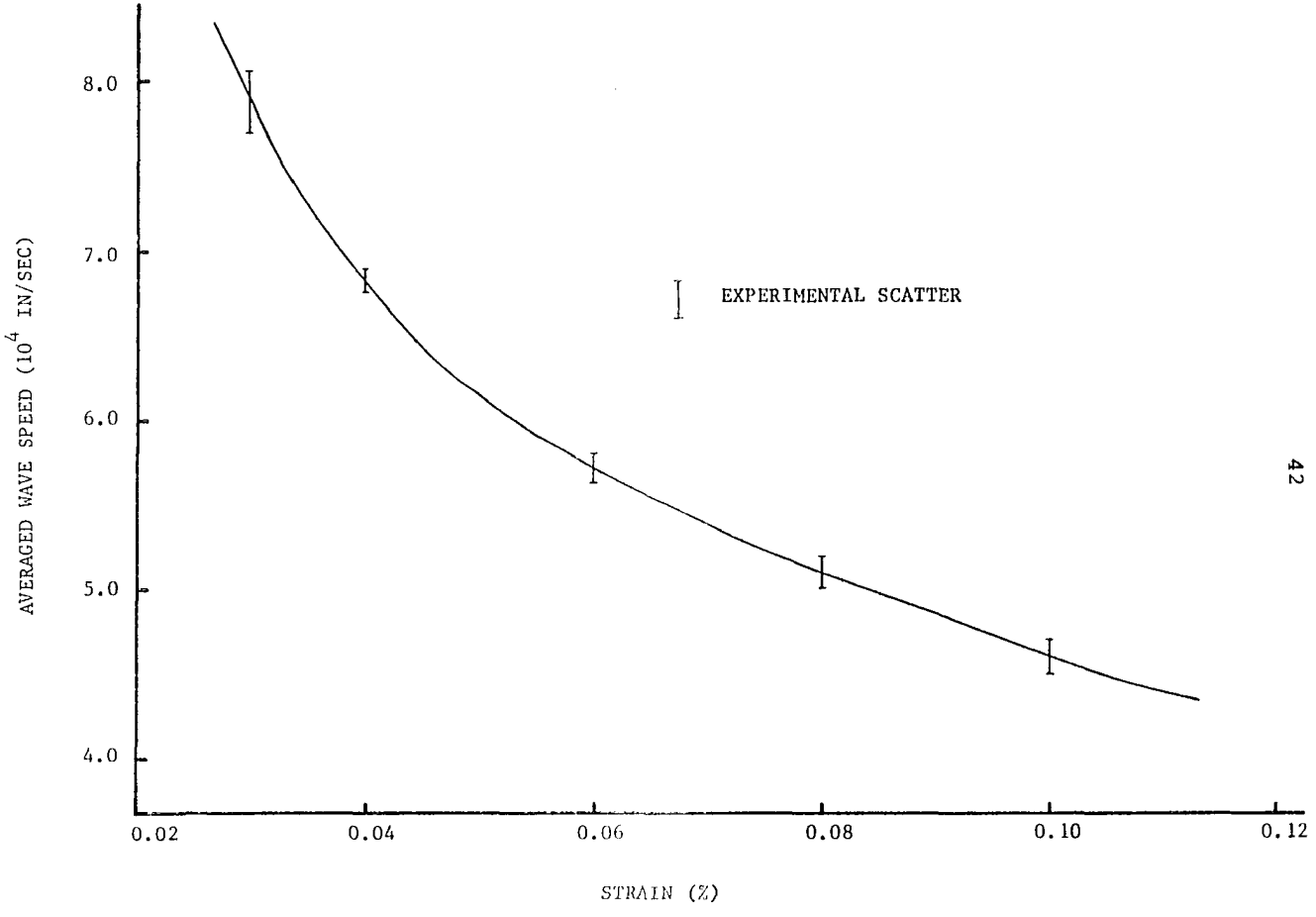

FIGURE 11. MEASURED AVERAGE WAVE SPEED VS STRAIN (BASED ON FIGURE 3).

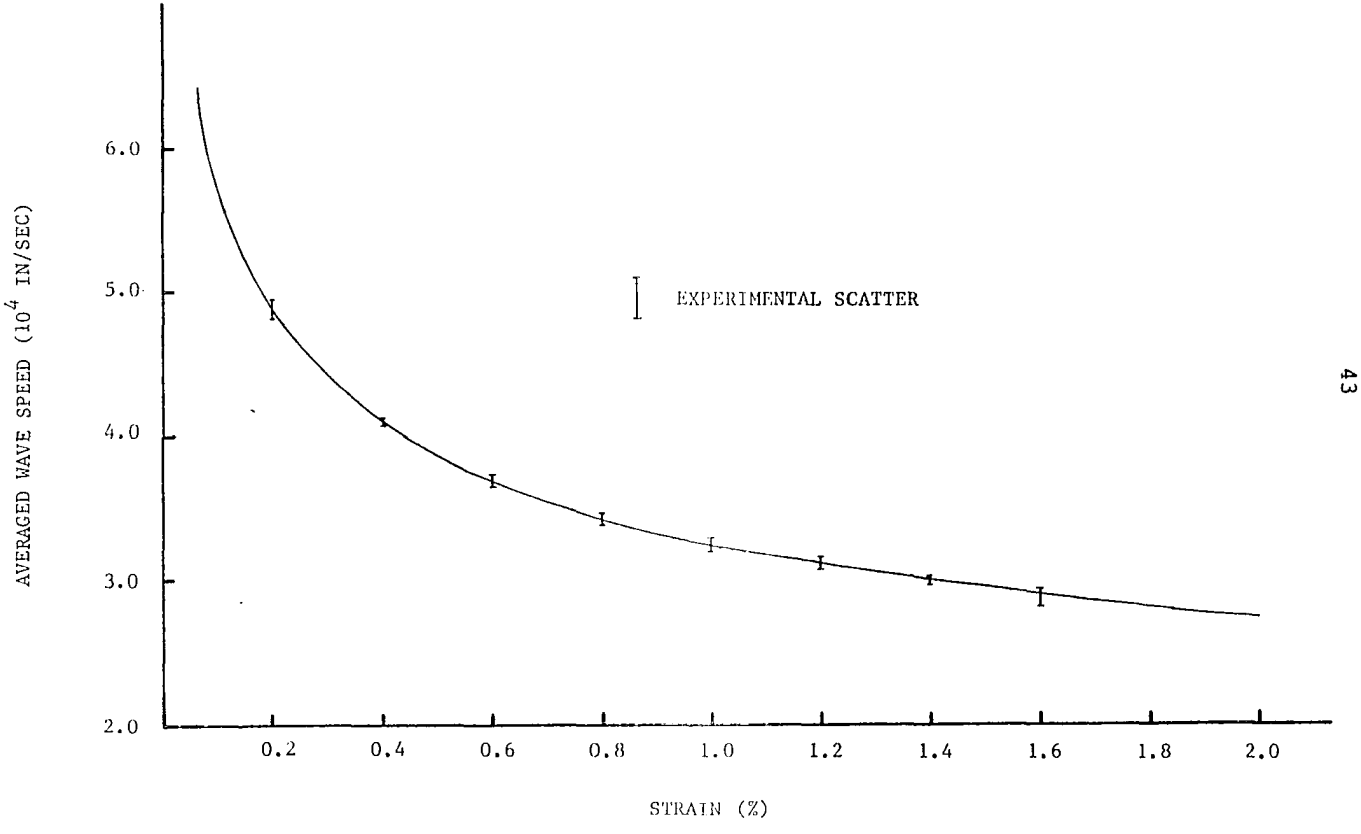

FIGURE 12. MEASURED AVERAGE WAVE SPEED VS STRAIN (BASED ON FIGURES 4 AND 5).

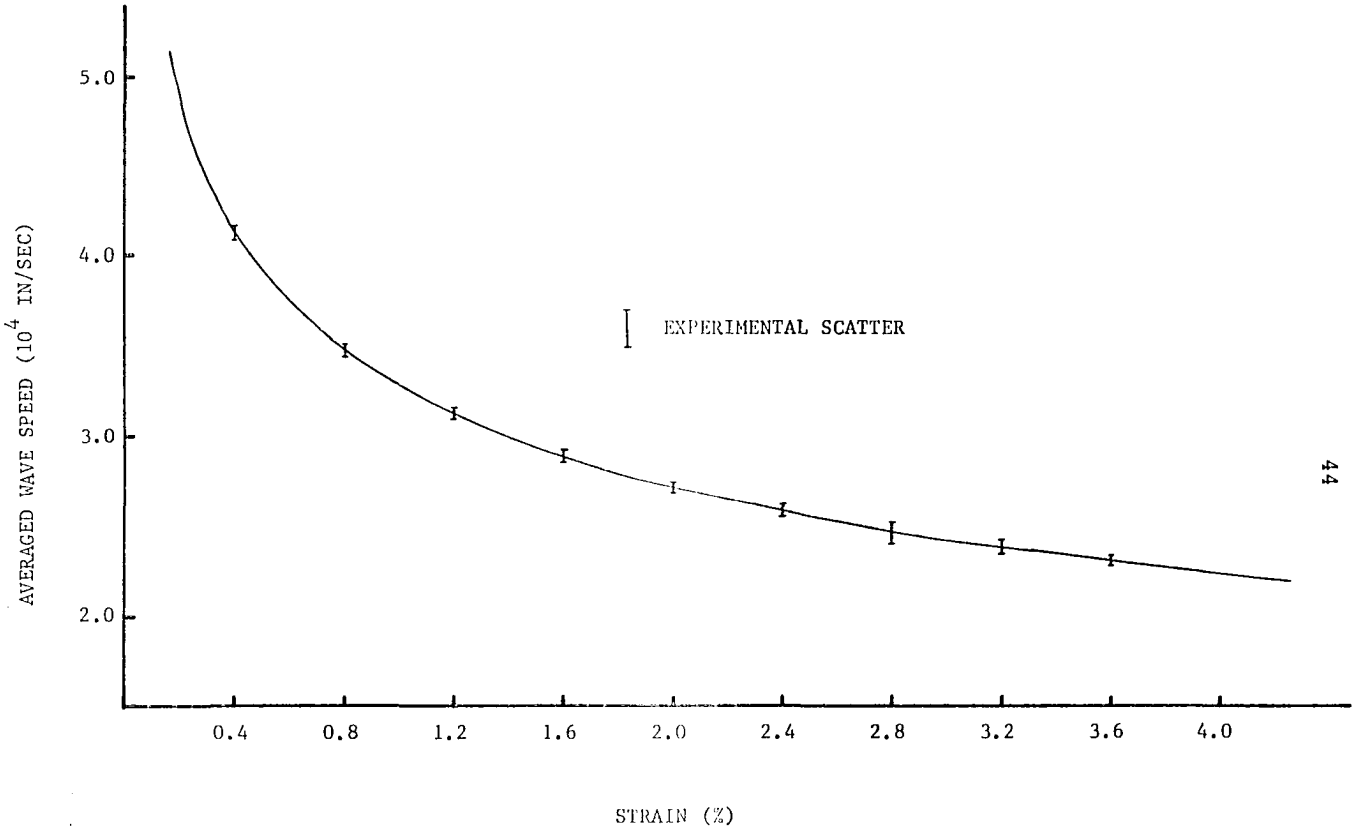

FIGURE 13. MEASURED AVERAGE WAVE SPEED VS STRAIN (BASED ON FIGURE 6).

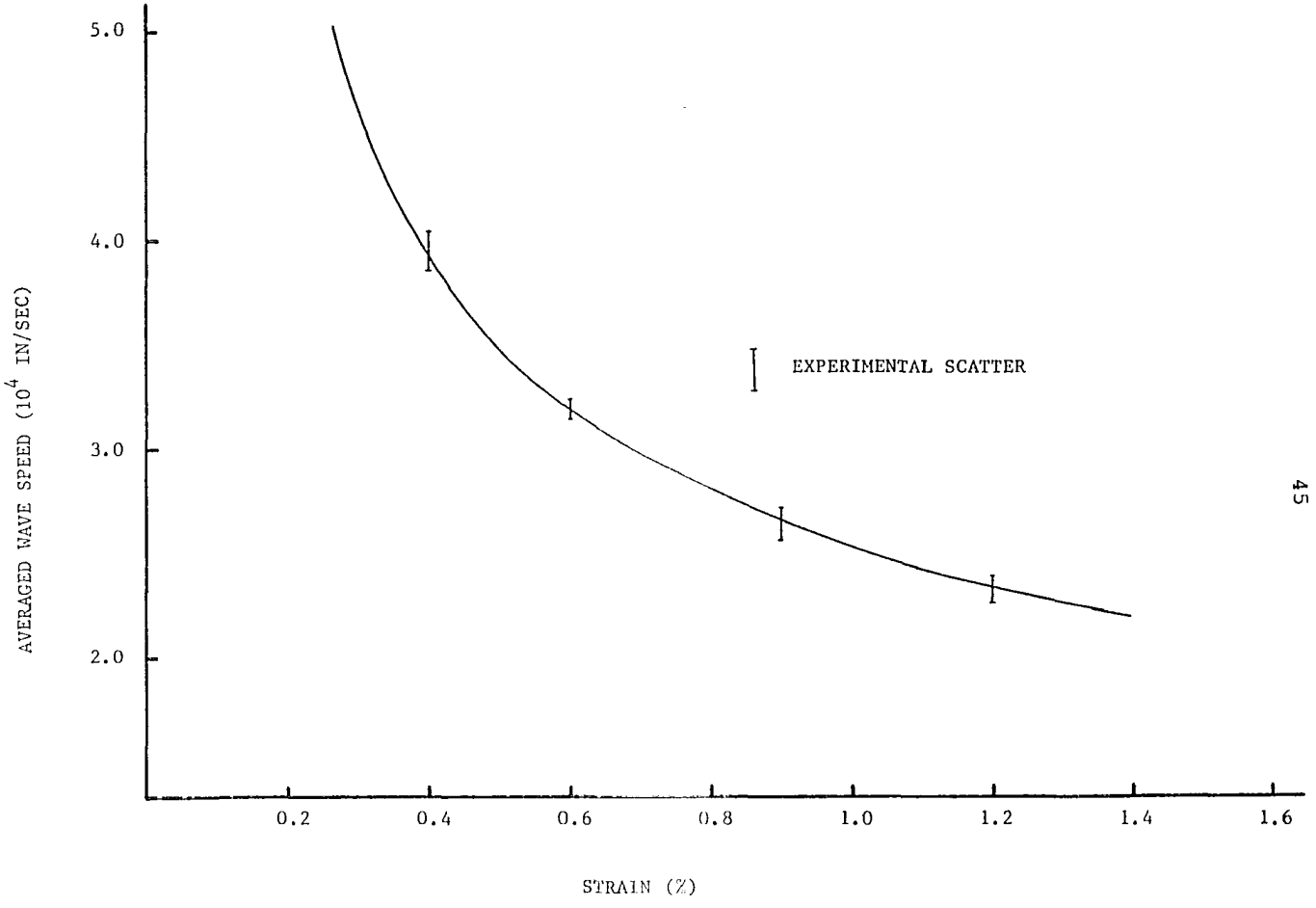

FIGURE 14. MEASURED AVERAGE WAVE SPEED VS STRAIN (BASED ON FIGURE 9).

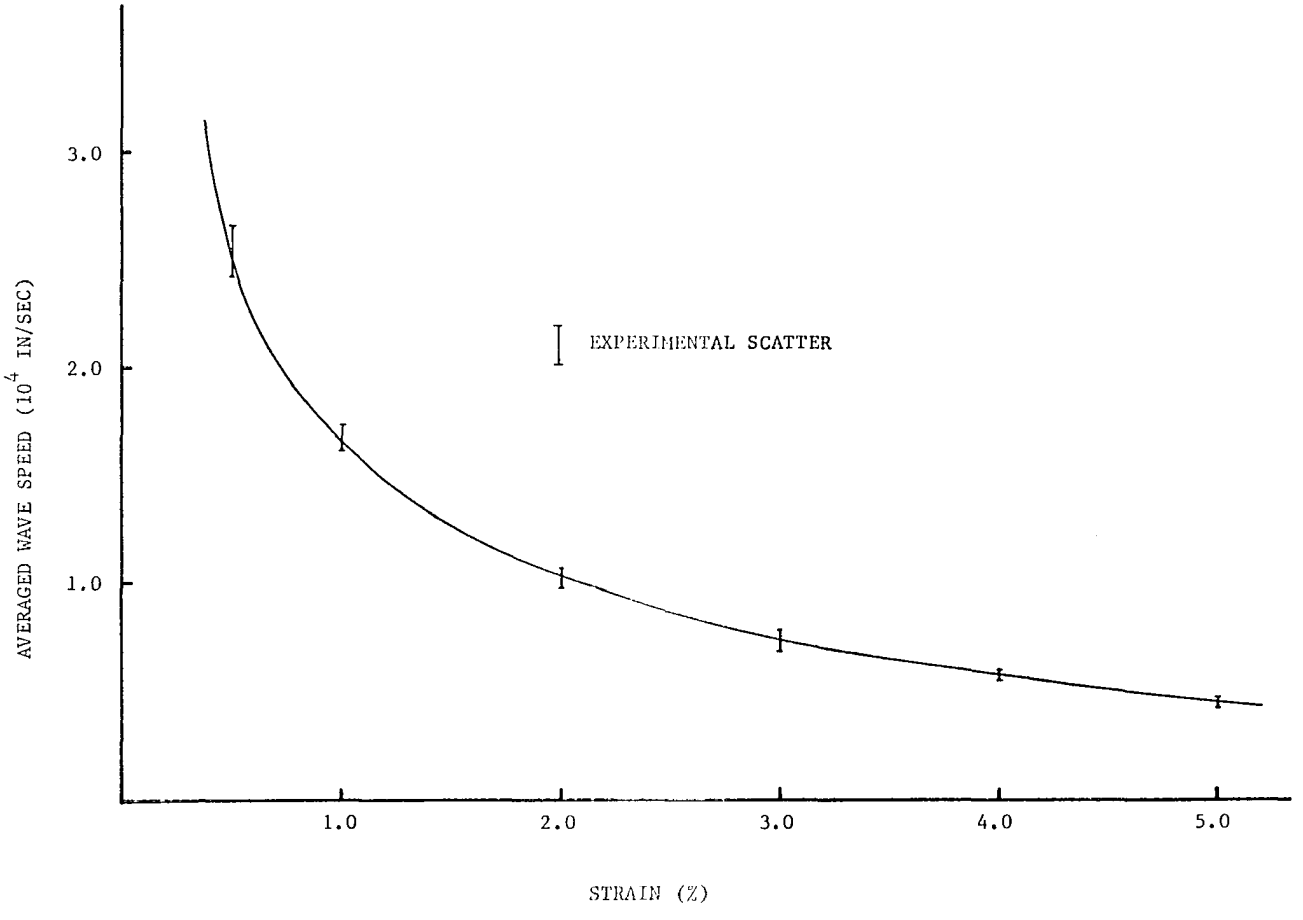

FIGURE 15. MEASURED AVERAGE WAVE SPEED VS STRAIN (BASED ON FIGURE 10).

4.4 Experimentally determined dynamic response function

A general power function equation was assumed:

$$\sigma - \sigma_Y = \beta (\epsilon - \epsilon_Y)^a \qquad (11)$$

where

σ = nominal axial stress

σ_Y = yield stress

ϵ = nominal axial strain

ϵ_Y = yield strain

β = the response function coefficient

a = the response function dimensionless exponent

Introducing eq. (11) into eq. (8) yields

$$C_p^2(\epsilon) = (\frac{a}{\rho}) \beta (\epsilon - \epsilon_Y)^{a-1} \qquad (12)$$

or

$$\beta = (\frac{\rho}{a}) C_p^2 (\epsilon - \epsilon_Y)^{1-a} \qquad (13)$$

Taking the logarithm of both sides of eq. (12) yields

$$\frac{\Delta \log (\epsilon - \epsilon_Y)}{\Delta \log C_p} = \frac{2}{a - 1} \qquad (14)$$

Figures 16 to 21 show that log-log plots of post-yield strain vs experimentally determined average wave speed.

The response function dimensionless exponent,a, was determined by the slope of such plots employing eq. (14). In Figures 16 and 19 to 21, the value of the slope was very close to -3 to give the exponent,a, a value of 1/3. Thus, the cubic response function was assumed. On the other hand, Figures 17 and 18 show that the value of the slope was sufficiently close to -4 to give the exponent, a, a value of 1/2, so that the parabolic function was assumed. The response function coefficient, β, was calculated by employing eq. (13) after the exponent,a, had been determined. Such calculations were shown in Tables 3 to 8. For fully annealed 1100-F aluminum and the condition of very low projectile velocity impact, the cubic dynamic response function was assumed with average coefficient β of 1.53×10^4 psi (10.72 Kg/mm^2); while for the conditions of moderate and high projectile velocity impact, the parabolic dynamic response function was assumed with average coefficient β of 5.312×10^4 psi (37.35 Kg/mm^2) and 5.272×10^4 psi (37.12 Kg/mm^2). For as received 1100-F aluminum and the conditions of low, moderate, and high projectile velocity (up to approximately 3000 in/sec) impact, only the cubic dynamic response

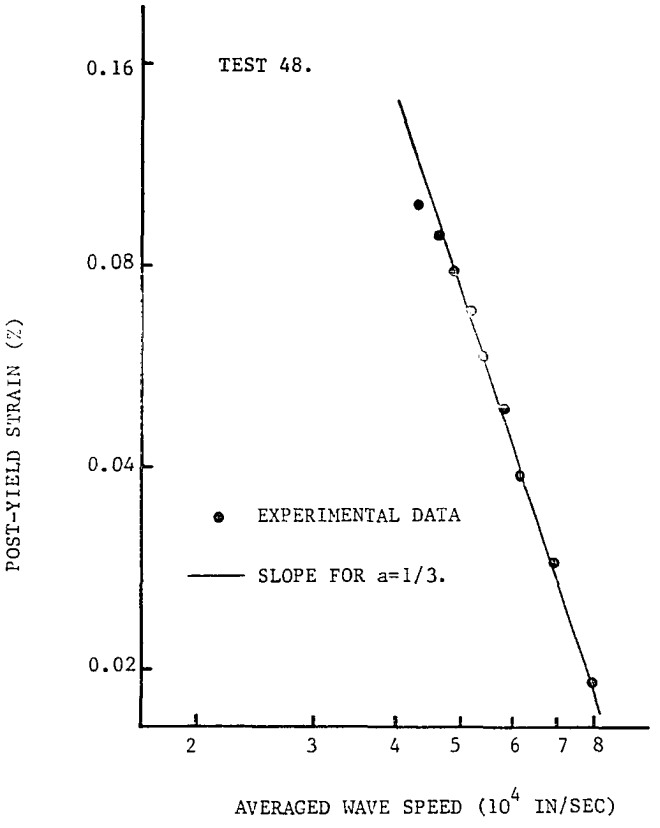

FIGURE 16. LOG-LOG PLOT OF POST-YIELD STRAIN VS AVERAGED WAVE SPEED (BASED ON FIGURE 3)

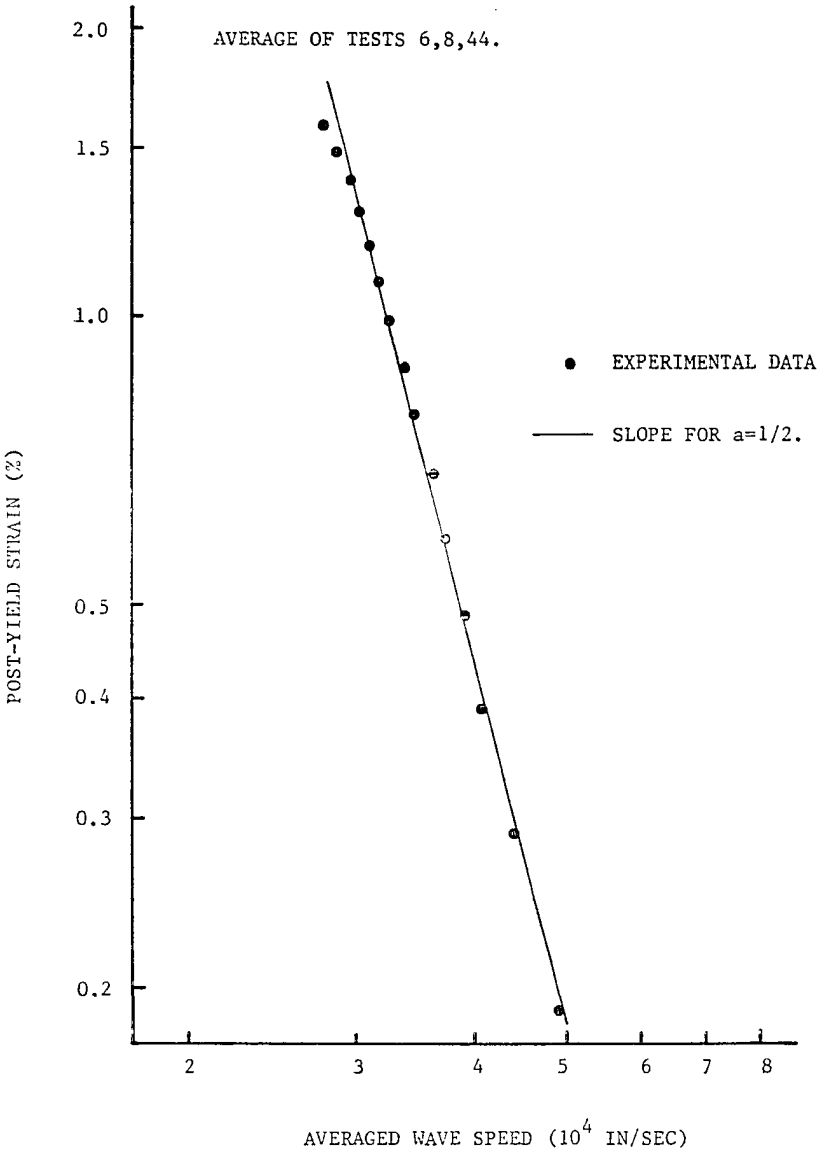

FIGURE 17. LOG-LOG PLOT OF POST-YIELD STRAIN VS AVERAGED WAVE SPEED (BASED ON FIGURE 4).

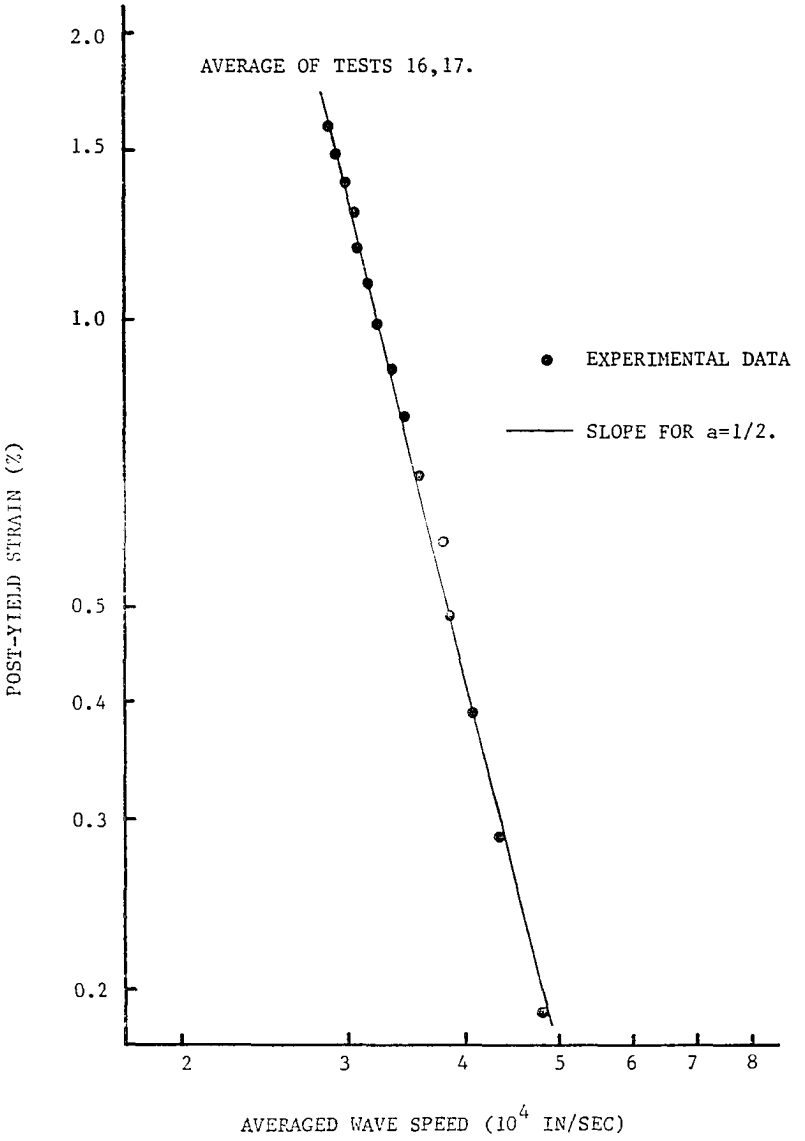

FIGURE 18. LOG-LOG PLOT OF POST-YIELD STRAIN VS AVERAGED WAVE SPEED (BASED ON FIGURE 5).

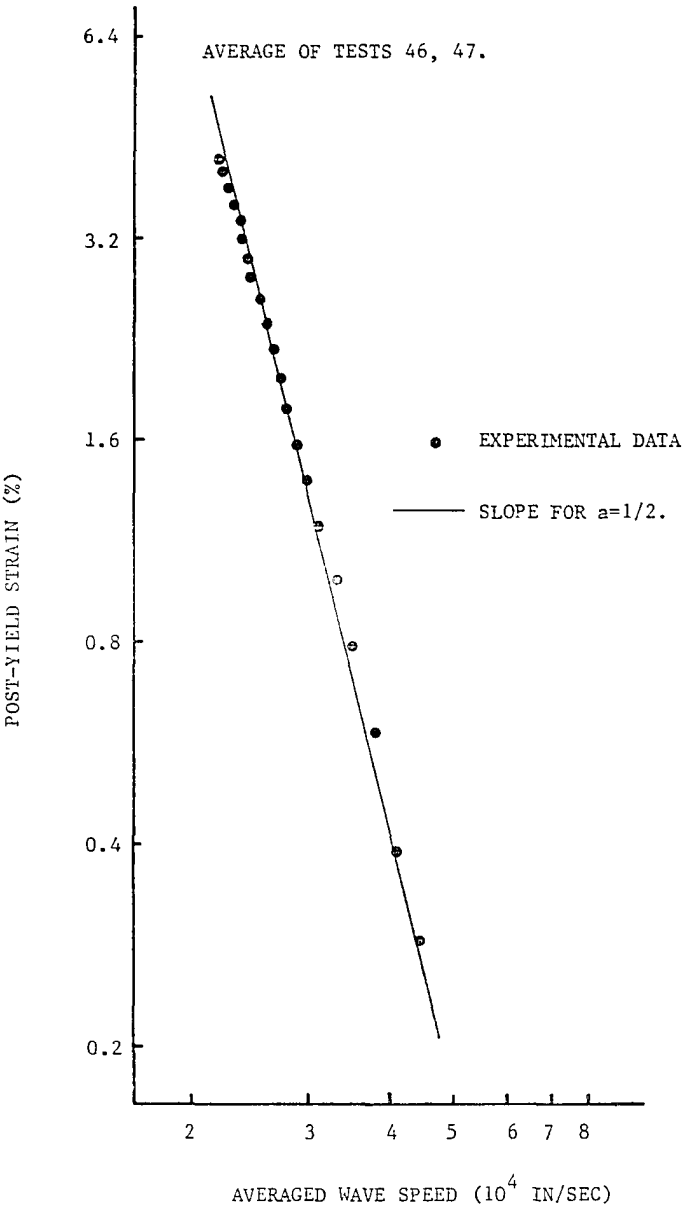

FIGURE 19. LOG-LOG PLOT OF POST-YIELD STRAIN VS AVERAGED WAVE SPEED (BASED ON FIGURE 6).

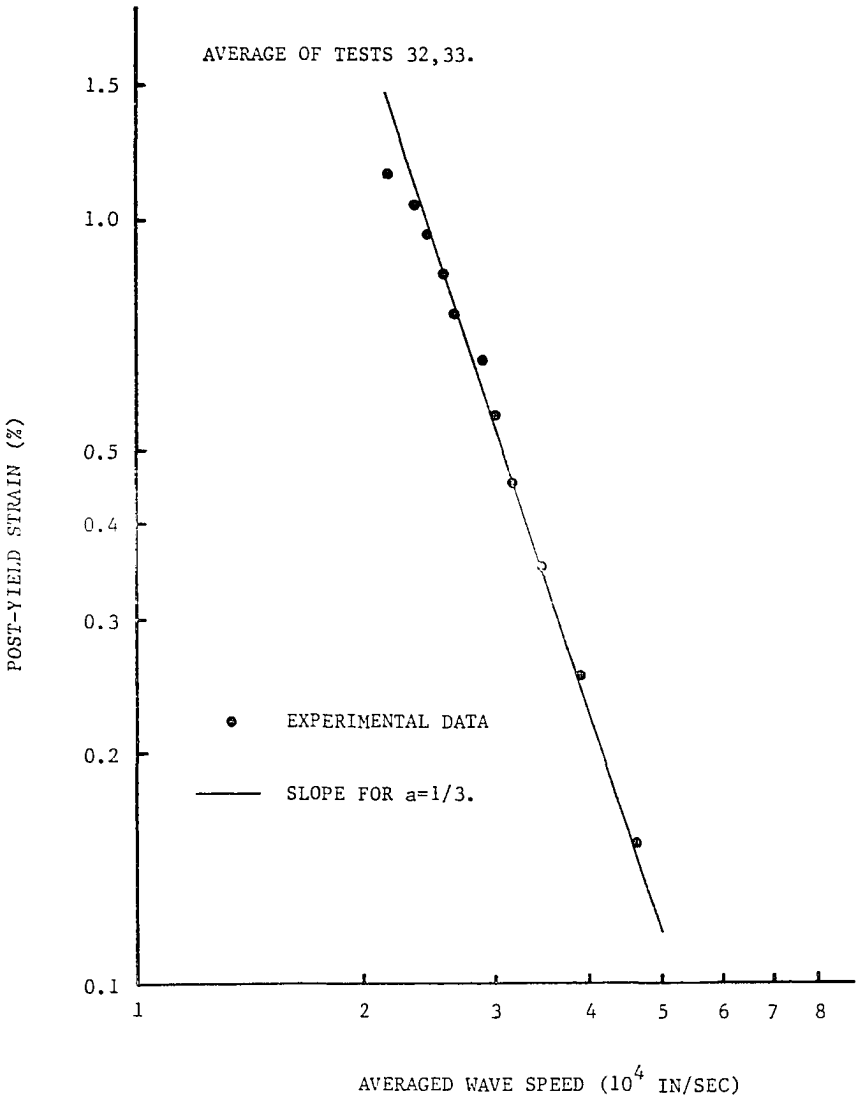

FIGURE 20. LOG-LOG PLOT OF POST-YIELD STRAIN VS AVERAGED WAVE SPEED (BASED ON FIGURE 9).

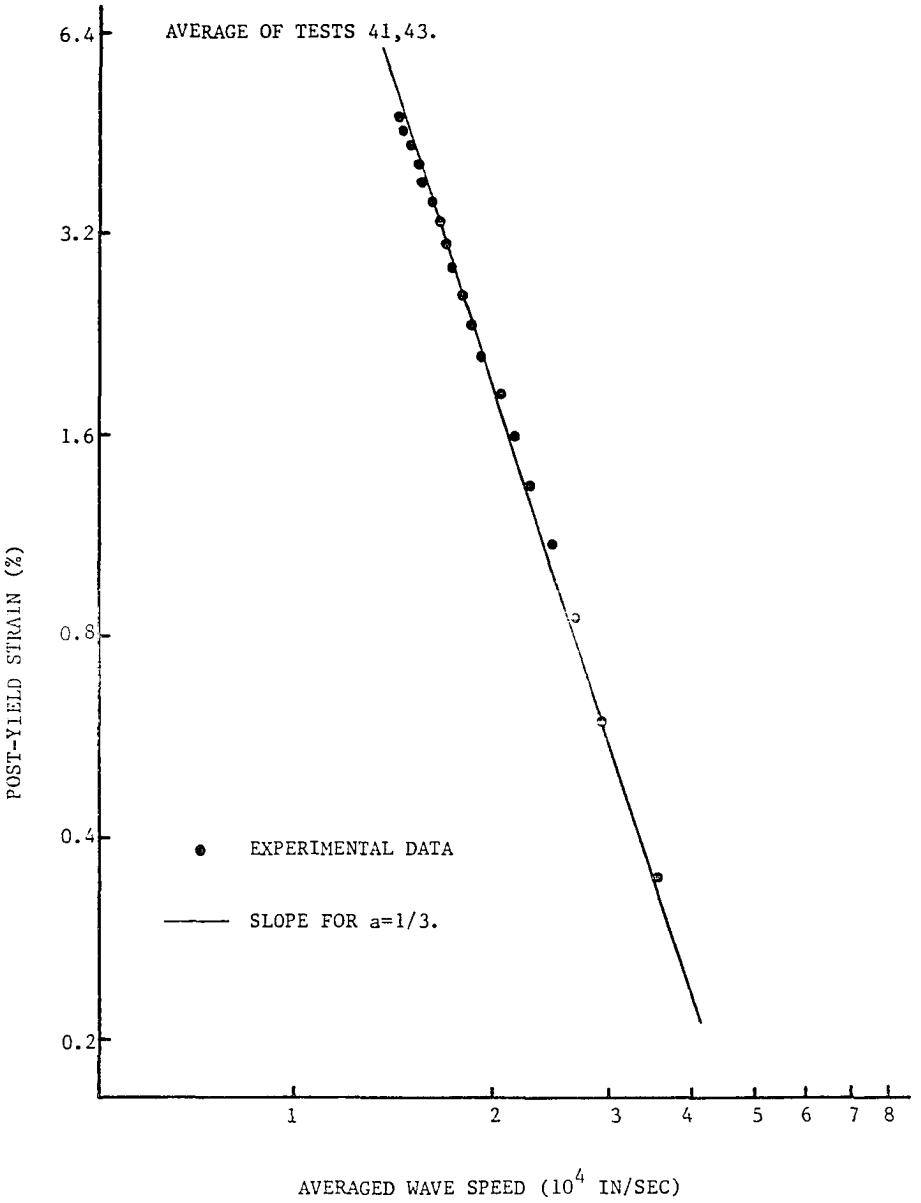

FIGURE 21. LOG-LOG PLOT OF POST- YIELD STRAIN VS AVERAGED WAVE SPEED (BASED ON FIGURE 10).

function was assumed. The average coefficient β in Table 6 was 2.07×10^4 psi (14.53 Kg/mm^2), while in Table 7 was 2.16×10^4 psi (15.22 Kg/mm^2).

The predicted wave arrival from one gage location to another using experimentally determined dynamic response function with their own coefficients were shown in Figures 3 to 10 except in Figures 7 and 8. The reason that the predicted plastic wave arrival was not be plotted in Figures 7 and 8 was because the plastic strain amplitudes were much lower than elastic strains such that the wave speeds could not be determined accurately.

4.5 Bell's empirical parabolic stress-strain law

Since 1956, by means of the then newly developed diffraction grating technique for measuring finite dynamic strain, Bell[45] discovered that the governing stress-strain function for each metal studied was

$$\sigma = \beta \epsilon^{\frac{1}{2}} \tag{15}$$

He showed that the parabola coefficient, β, is linearly dependent on the temperature and proportional to the zero-

point isotropic elastic modulus $\mu(0)$ multipled by a dimensionless universal constant $B_o = 0.0280$. The deformation mode is designated by a discrete factor $(\frac{2}{3})^{\frac{r}{2}}$ where r is an integer. Thus, the expression of β is as follows:

$$\beta = (\frac{2}{3})^{\frac{r}{2}} \mu(0) B_o (1 - \frac{T}{T_m}) \qquad (16)$$

where T, T_m are the test temperature and melting point temperature of the material, respectively.

For polycrystalline 1100-F fully annealed aluminum at room temperature ($300^{\circ}K$) β is 5.60×10^4 psi ($39.4\ Kg/mm^2$).

4.6. Quasi-static tests

A quasi-static uniaxial simple compression test was performed for 'fully annealed' as well as 'as received' 1100-F aluminum in order to compare response function with impact dynamic measurements. Detailed quasi-static nominal or engineering stress-strain curves for those two types of 1100-F aluminum are shown in Figures 22 to 24. For fully annealed 1100-F aluminum, the initial portion of the loading curve was linear, and the yield point was

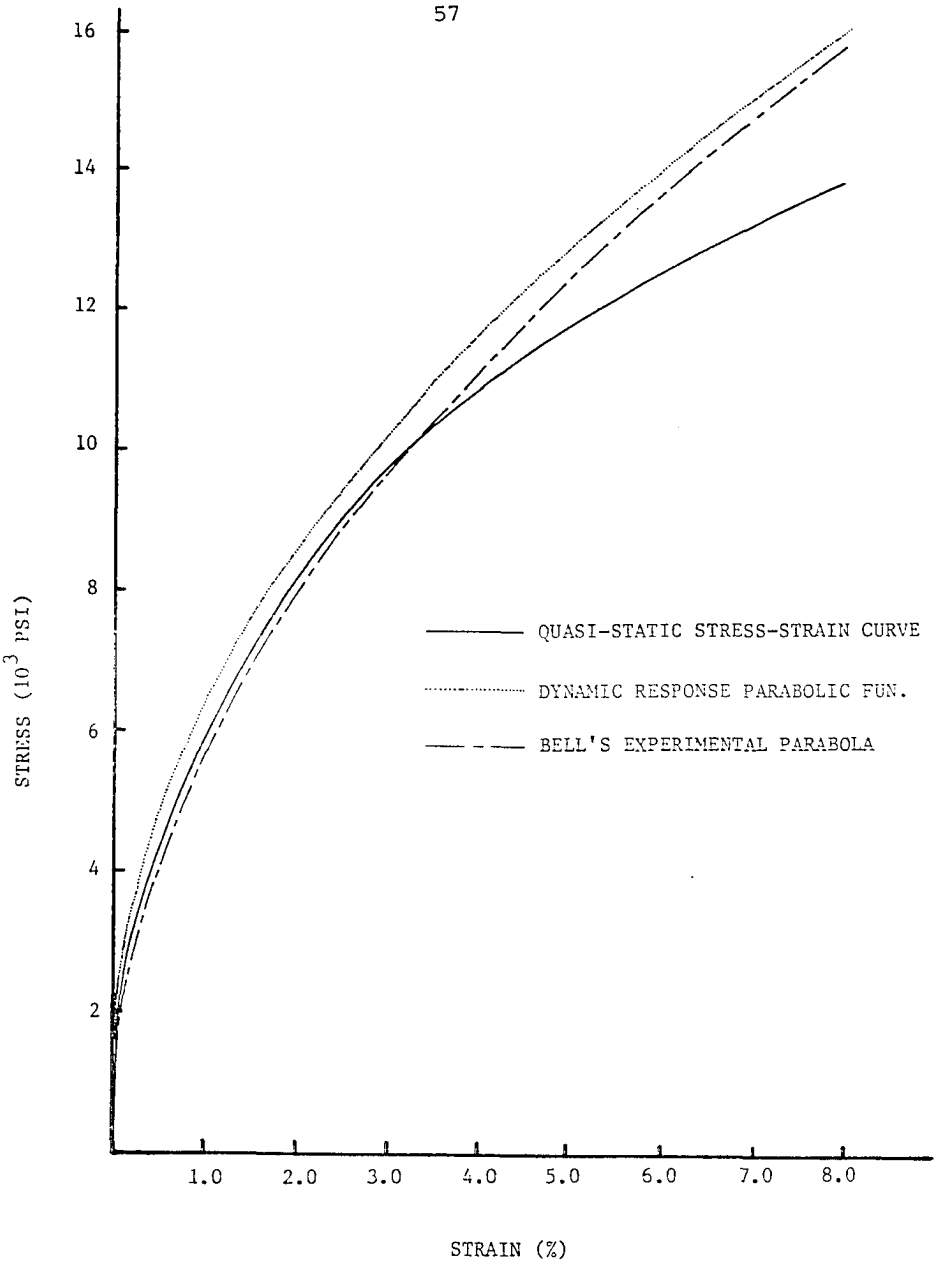

FIGURE 22. A COMPARISON OF THE EXPERIMENTALLY DETERMINED DYNAMIC RESPONSE PARABOLIC FUNCTION, BELL'S EXPERIMENTAL PARABOLA, AND QUASI-STATIC STRESS-STRAIN CURVE FOR FULLY ANNEALED 1100-F ALUMINUM.

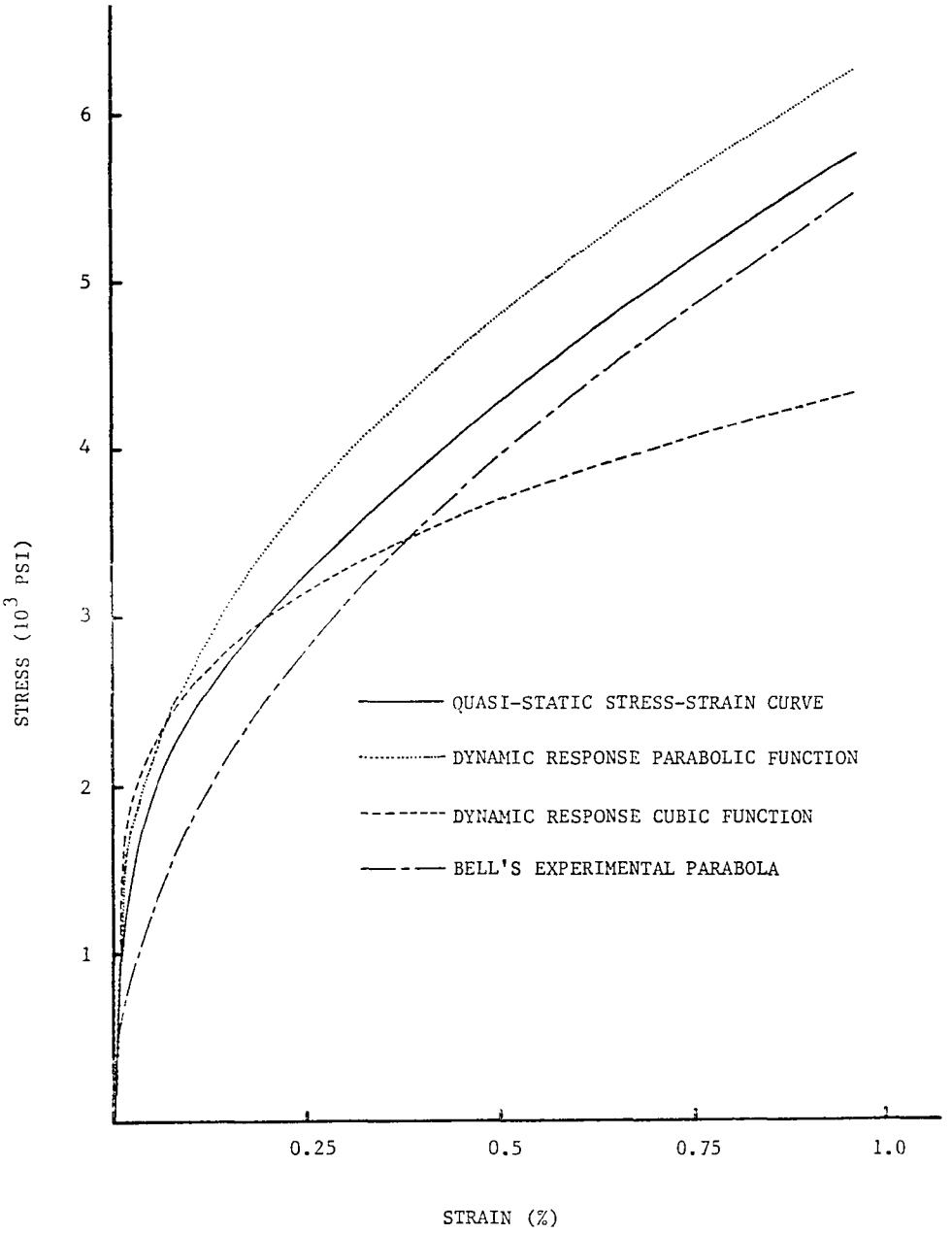

FIGURE 23. A COMPARISON OF THE EXPERIMENTALLY DETERMINED DYNAMIC RESPONSE FUNCTION (PARABOLIC AND CUBIC), BELL'S EXPERIMENTAL PARABOLA AND QUASI-STATIC CURVE FOR FULLY ANNEALED 1100-F ALUMINUM.

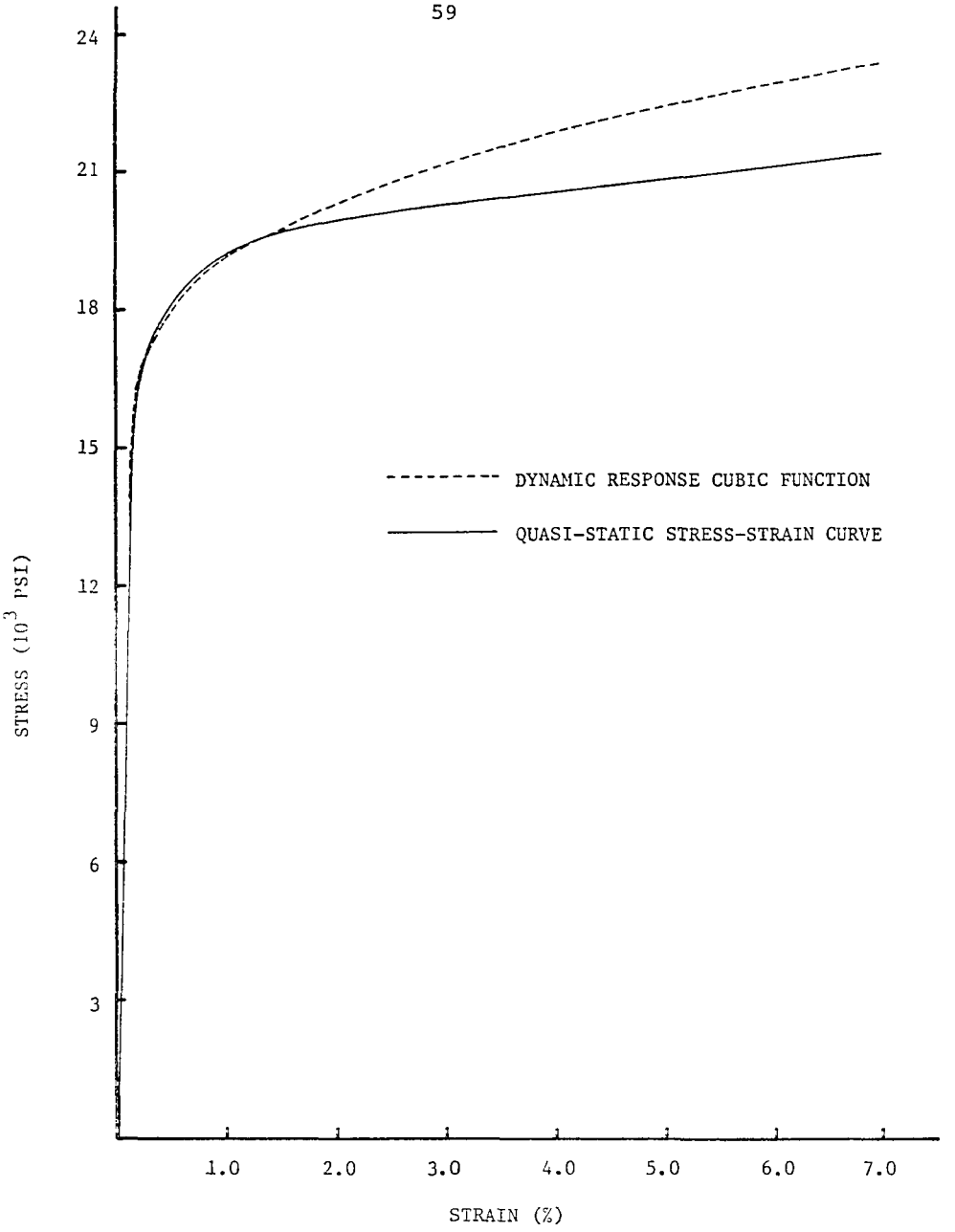

FIGURE 24. A COMPARISON OF THE EXPERIMENTALLY DETERMINED DYNAMIC RESPONSE CUBIC FUNCTION AND QUASI-STATIC STRESS-STRAIN CURVE FOR AS-RECEIVED 1100-F ALUMINUM.

very close to 1100 psi (0.77 Kg/mm^2) stress and 0.011% strain. Employing the uniaxial linear stress-strain function, the Young's modulus,E, at room temperature was 10 x 10^6 psi (7030 Kg/mm^2). Square post-yield nominal stress vs nominal strain were plotted in Figures 25 and 26. The composite curve which represents the quasi-static stress-strain curve up to six percent strain may be divided into four regions. The constitutive equations which describe the quasi-static compression data extended to six percent strain for this fully annealed 1100-F aluminum are expressed as follows:

In the elastic region, $0 \leqslant \epsilon \leqslant 0.011\%$,

$$\sigma = E\,\epsilon \quad \text{with} \quad E = 10 \times 10^6 \text{ psi} \tag{17}$$

In the region, $0.011\% < \epsilon \leqslant 0.4\%$,

$$\sigma - \sigma_Y = \beta(\epsilon - \epsilon_Y)^{\frac{1}{2}} \text{ with } \beta = 4.27 \times 10^4 \text{ psi} \tag{18}$$

In the region, $0.4\% < \epsilon \leqslant 3.0\%$,

$$\sigma - \sigma_Y = \beta(\epsilon - \epsilon_Y)^{\frac{1}{2}} \text{ with } \beta = 5.15 \times 10^4 \text{ psi} \tag{19}$$

In the region, $3.0\% < \epsilon \leqslant 6.0\%$,

$$\sigma - \sigma_Y = \beta(\epsilon - \epsilon_Y)^{\frac{1}{2}} \text{ with } \beta = 4.408 \times 10^4 \text{ psi} \tag{20}$$

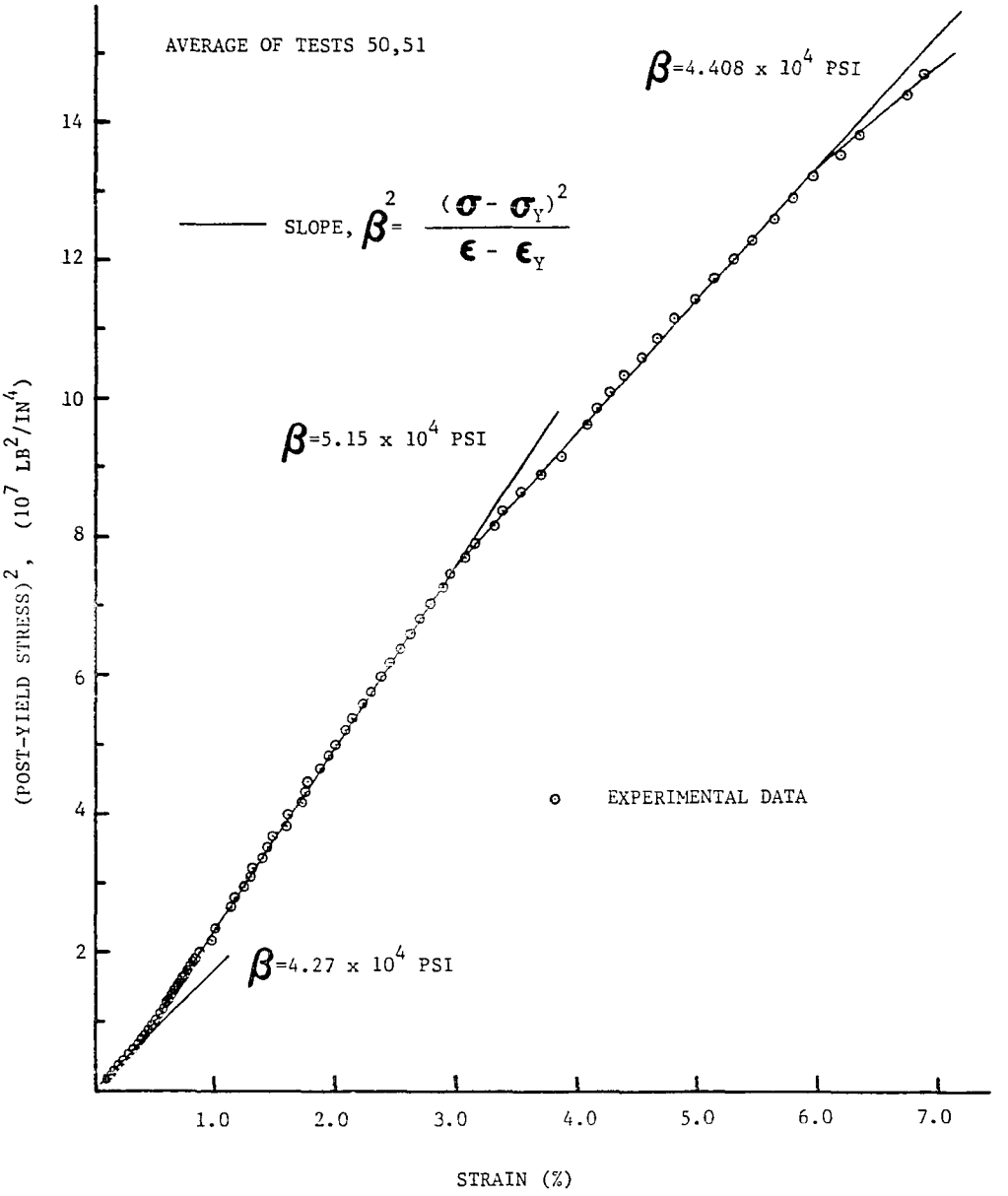

FIGURE 25. POST-YIELD STRESS SQUARED VS STRAIN FOR QUASI-STATIC UNIAXIAL COMPRESSION TEST IN FULLY ANNEALED 1100-F ALUMINUM.

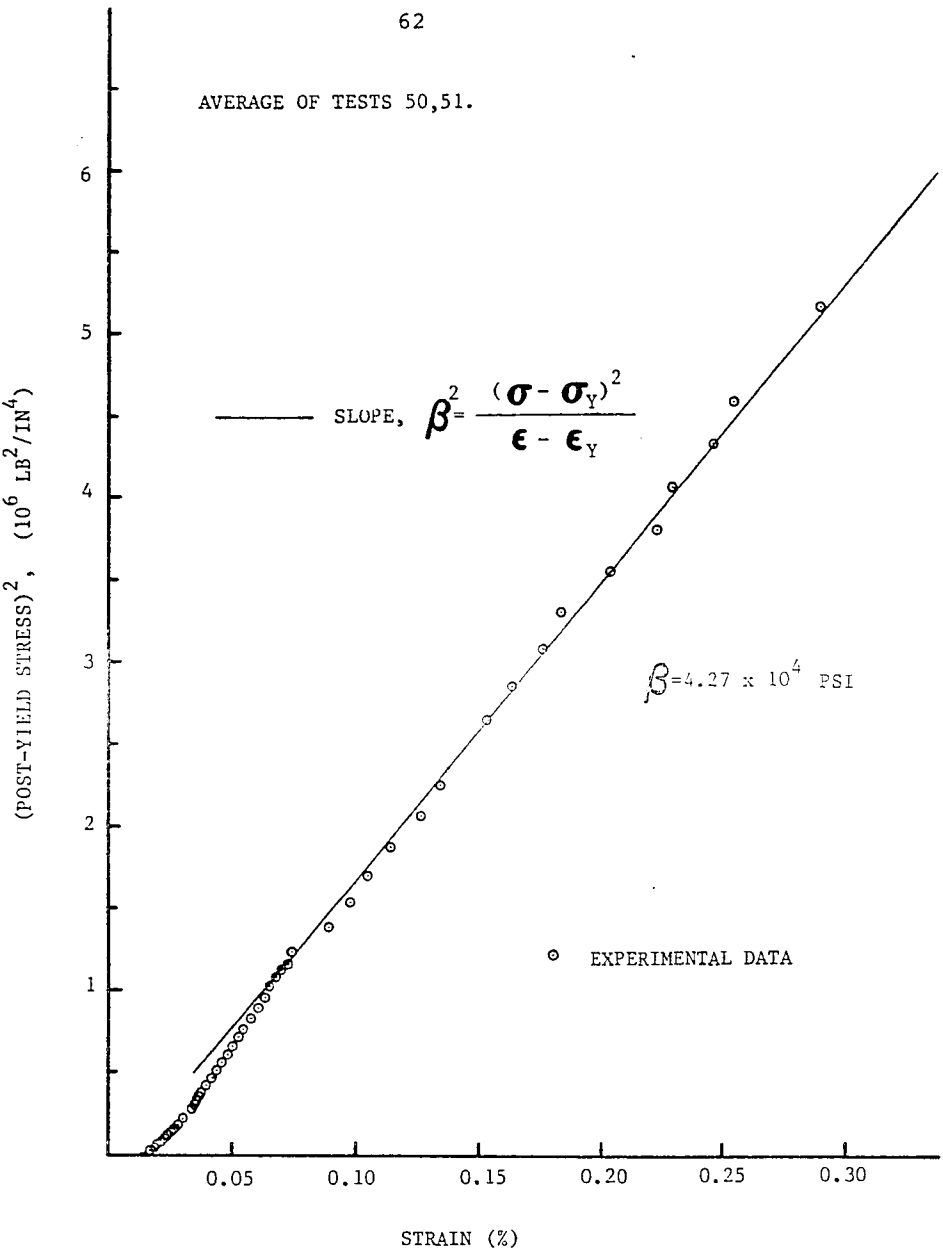

FIGURE 26. POST-YIELD STRESS SQUARED VS STRAIN FOR QUASI-STATIC UNIAXIAL COMPRESSION TEST IN FULLY ANNEALED 1100-F ALUMINUM.

For as received 1100-F aluminum, the yield point was observed to be close to 13,600 psi (9.56 Kg/mm^2) stress and 0.136% strain. Cubic post-yield nominal stress vs nominal strain was plotted in Figure 27. The composite curve which describe the quasi-static stress-strain curve up to seven percent strain may be divided into four regions. The constitutive equations for describing this quasi-static data are summarized as follows:

In the elastic region, $0 < \epsilon \leq 0.136\%$,

$$\sigma = E\epsilon \qquad \text{with } E = 10 \times 10^6 \text{ psi} \tag{21}$$

In the region, $0.136\% \leq \epsilon \leq 0.65\%$,

$$\sigma - \sigma_Y = \beta(\epsilon - \epsilon_Y)^{1/3} \text{ with } \beta = 2.75 \times 10^4 \text{ psi} \tag{22}$$

In the region, $0.65\% < \epsilon \leq 1.3\%$,

$$\sigma - \sigma_Y = \beta(\epsilon - \epsilon_Y)^{1/3} \text{ with } \beta = 2.30 \times 10^4 \text{ psi} \tag{23}$$

In the region, $1.3\% < \epsilon \leq 7.0\%$,

$$\sigma - \sigma_Y = \beta(\epsilon - \epsilon_Y)^{1/3} \text{ with } \beta = 1.66 \times 10^4 \text{ psi} \tag{24}$$

4.7. A comparison of observed experimental maximum strain and predicted values

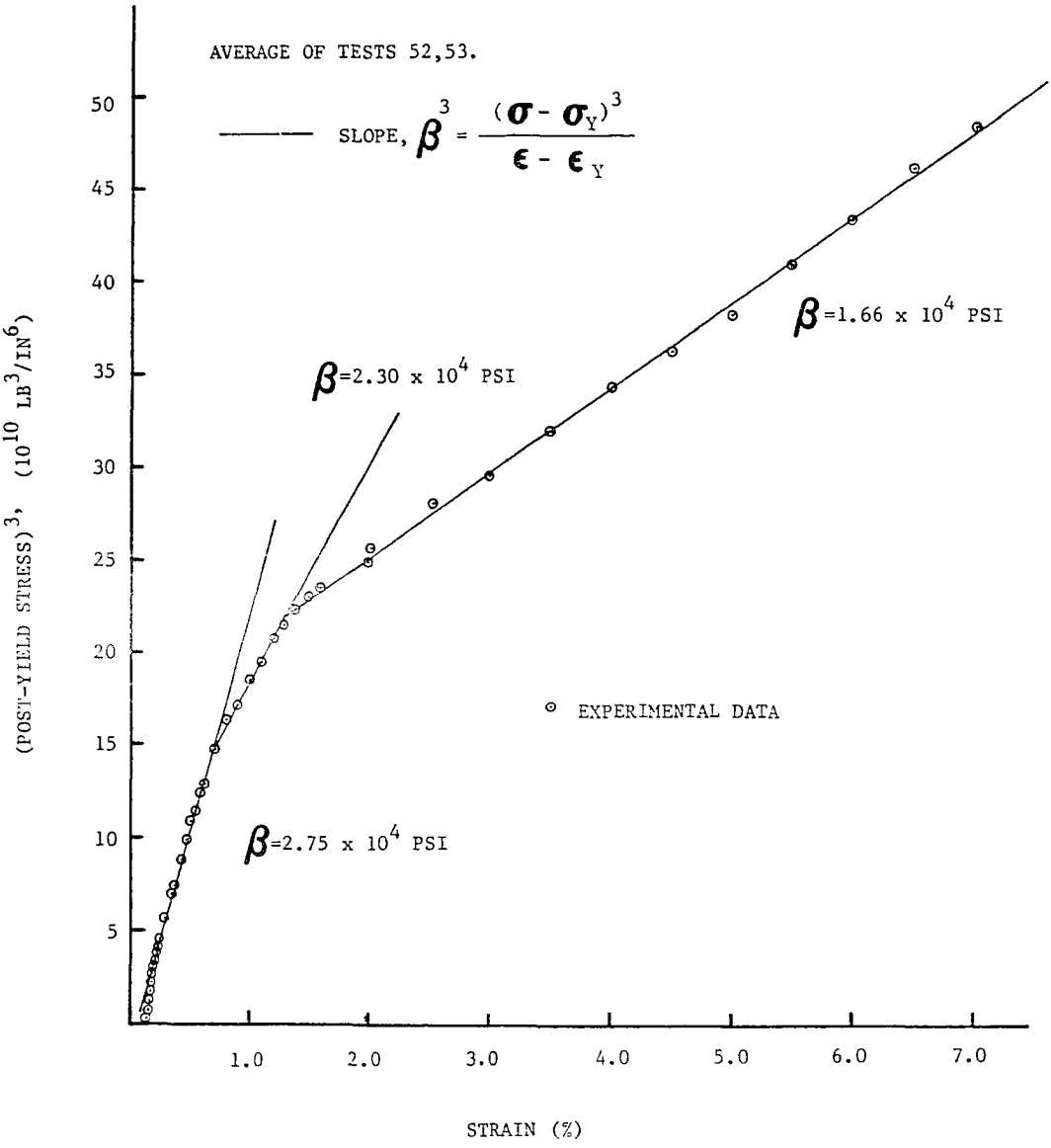

FIGURE 27. POST-YIELD STRESS CUBE VS STRAIN FOR QUASI-STATIC UNIAXIAL COMPRESSION TEST IN AS-RECEIVED 1100-F ALUMINUM.

In subsection (4.4), the formulation of the experimentally determined dynamic response function has been described in detail. In the following, those functions are summarized:

For fully annealed 1100-F aluminum, in the level of strain amplitude is around or slightly above the yield strain,

$$\sigma - \sigma_Y = \beta(\epsilon - \epsilon_Y)^{1/3} \quad \text{with } \beta = 1.53 \times 10^4 \text{ psi} \tag{25}$$

Other level of strain amplitude up to 5%,

$$\sigma - \sigma_Y = \beta(\epsilon - \epsilon_Y)^{1/2} \quad \text{with the net average value } \beta = 5.292 \times 10^4 \text{ psi} \tag{26}$$

For as received 1100-F aluminum, in the level of strain amplitude up to 6%,

$$\sigma - \sigma_Y = \beta(\epsilon - \epsilon_Y)^{1/3} \quad \text{with } \beta = 2.115 \times 10^4 \text{ psi} \tag{27}$$

Once the response function parameters β and a are determined, introducing the assumed general power function eq. (11) into eqs. (8) and (9), one obtains

$$V_{max}^2 = \left(\frac{E}{\rho}\right)^{\frac{1}{2}} \epsilon_Y + \frac{a\beta}{\rho}\left(\frac{2}{a+1}\right)^2 \left(\epsilon_{max} - \epsilon_Y\right)^{a+1} \tag{28}$$

Since the mechanical impedances of the specimen and projectile are the same, the equivalence of stress and particle velocity at the impact face causes a jump in the magnitude of the particle velocity of the specimen equal to half of the projectile velocity. i.e. $V_{max} = \frac{1}{2} V_{projectile}$. The density of 1100-F aluminum is 2.53×10^{-4} lb-sec^2/in^4 (2.75×10^2 Kg-sec^2/m^4). Table 9 gives a comparison of observed experimental and predicted maximum strain. The predicted values are obtained from eq.(28) employing the experimentally determined dynamic response function, Bell's experimental parabola, and quasi-static curves. The excellent agreement of observed and predicted maximum strain using experimentally determined dynamic response function shows that eq. (2) holds and demonstrates the applicability of the strain-rate-independent finite-amplitude wave theory. As may be seen in Table 9, the observed maximum strain is in very good agreement with predictions from Bell's experimental parabola and in fair agreement with those from the slopes of the quasi-static

stress-strain curve. As shown in Figures 22 and 23, in the fully annealed 1100-F aluminum, maximum strains did not exceed 3.5 percent, which is a region with slopes approximately close to the slopes of response parabolic function, Bell's parabola, and quasi-static curves. For this reason, the predicted values of maximum strain are in agreement with observed maximum strain. In the region of very low strain, the dynamic results follow the response cubic function rather than the response parabolic function. As Bell pointed out, in this region of low strain, in using his experimental parabola, proper allowance must be made for the initial elastic limit. Thus, below strains of almost 3.5 percent the quasi-static stress-strain curve is somewhat higher than Bell's parabola. In the region over 3.5 percent, as may be seen from Figure 22, the slopes of response parabolic function or Bell's parabola are quite different than those of quasi-static curve; thus, one may no longer use the quasi-static curve to predict the wave propagation. It becomes obvious that only the experimentally determined dynamic response function governed the dynamic deformation at all level of strains, not the quasi-static curve. The dynamic results may follow Bell's

parabola, but not better than the dynamic response functions developed in this study. Figure 24 shows a comparison of the experimentally determined dynamic response cubic function and quasi-static stress-strain curve for as received 1100-F aluminum. The maximum strains between the experimental results and those predicted values have been compared in Table 9. From the overall comparison, the dynamic response cubic function indeed governed the dunamic deformation at maximum strain up to six percent.

Table 9

A COMPARISON OF OBSERVED AND PREDICTED MAXIMUM STRAINS

MATERIAL	FULLY ANNEALED 1100-F AL.				AS RECEIVED 1100-F AL.			
TEST NO.	48	6,8,44	16,17	46,47	28	30	32,33	41,43
AVERAGE PROJECTILE VELOCITY, IN/SEC	221	1637	1651	2862	702	653	1622	2811
DISTANCE OF GAGE LOCATION FROM IMPACT FACE, IN	1	1	1	1	1/2	1/2	1/2	1/2
OBSERVED MAX. STRAIN, %	0.160	2.19	2.25	4.86	0.22	0.19	1.92	5.72
PREDICTED MAX. STRAIN FROM DYNAMIC RESPONSE FUN. EQS. (25),(26) & (27), %	0.162	2.27	2.30	4.86	0.21	0.17	1.82	5.41
PREDICTED MAX. STRAIN FROM QUASI-STATIC CURVE, EQS. (17) to (24), %	0.151	2.39	2.42	5.21	0.19	0.16	1.60	5.72
PREDICTED MAX. STRAIN FROM BELL'S EXP. PARABOLA, EQ. (15), %	0.157	2.27	2.29	4.77				

CHAPTER V

SUMMARY AND CONCLUSIONS

The purpose of this study was to make direct and comprehensive experiments related to the finite-amplitude wave theory in 'fully annealed' as well as 'as received' 1100-F aluminum. Three levels of strain amplitude due to one-dimensional stress waves were observed in solid cylinder and tubular specimens by constant-velocity free flight symmetrical impact. The lower level of strains are around and slightly above the yield strain, while intermediate and high levels of strain are much higher than the yield strain. The measured wave speed and dynamic yield strain have been used to determine a dynamic response function. The experimental data have shown that the dynamic response function is cubic in as received 1100-F aluminum and is parabolic (except at the lower levels of strain) in fully annealed 1100-F aluminum. All the experimental

measurements have shown the applicability of one-dimensional strain-rate-independent theory of finite-amplitude waves in fully annealed and as received 1100-F aluminum.

The experimentally determined dynamic response functions obtained by the direct measurement of dynamic strain profiles, showed that the governing stress-strain relation can be divided into two types: parabolic and cubic. However, in research on finite-strain plasticity, Moon[45] and Bell[46,47] have shown some fascinating revelations about the existence of a yield region bounded by inner and outer yield surfaces. The dynamic yield point used in this paper is believed to be a point on the inner yield surface. The deformation below the inner or lower yield limit is predominately elastic, while beyond the outer or higher yield limit it is predominately plastic. Between the two limits, partially plastic deformation occurs. Bell's diffraction grating measurements of strain in as received 1100-F aluminum, approximately the same material used in this study, have shown that the dynamic outer yield stress for this material

is 165.52 MPa (24,000 psi). The corresponding strain at the dynamic outer yield stress 24,000 psi employing eq. (27) is 8.38 percent. Thus, all the three levels of strain profiles in as received 1100-F aluminum are located in the yielding region which is the region between inner and outer yield limit. The dynamic response cubic function governed the stress-strain law in the yielding region. For fully annealed 1100-F aluminum, there is no available data of dynamic outer yield point, but the existence of an outer yield strain based on quasi-static test has been found to be 0.07 percent strain. Therefore, the low level of strain profile (0.16 percent maximum strain) in fully annealed 1100-F aluminum is near the yielding region, and the dynamic response cubic function is formulated. The two other levels of strain profile are much above outer yield point. Thus, a dynamic response parabolic function is determined.

REFERENCES

1. Hopkinson, J. "On the Rupture of Iron Wire by a Blow," Proceedings of the Machester Literary and Philosophical Society, 11, 40-45, 1872 (or see Reference 3).

2. Dunn, B., "A Photographic Impact Testing Machine for Measuring the Varying Intensity of an Impulsive Force," J. Franklin Inst., 144(5), 321-348, 1897 (or see Reference 3).

3. Bell, J.F., "The Experimental Foundations of Solid Mechanics," Handbuch der Physik, Vol. VIa/1, Springer-Verlag, Berlin, 1973.

4. Clifton, R.J., "Plastic Waves: Theory and Experiment," Mechanics Today, 1, ed. by Nemat-Nasser, S., 102-167, Pergamon, 1972.

5. Manjoine, M.J. and Nadai, A.L., "High-Speed Tension Tests at Elevated Temperatures," Proc. Am. Soc., Testing Materials, 40, 822-839, 1940.

6. Kolsky, H., "An Investigation of the Mechanical Properties of Materials at Very High Rates of Loading," Proc. Phys. Soc. (London), B62, 676-700, 1949.

7. Campbell, W.R., "Determination of Dynamic Stress-Strain Curves from Strain Waves in Load Bars," U.S. Nat. Bur. Std. Rep. No. 1017, 1951.

8. Bell, J.F., "Determination of Dynamic Plastic Strain Through the Use of Diffraction Gratings," J. Appl. Phys., 27(10), 1109-1113, 1956.

9. Malvern, L.E., "Experimental Studies of Strain-Rate Effects and Plastic-Wave Propagation in Annealed Aluminum," Proc. of Behavior of Materials Under Dynamic Loading, ed. by N.J. Huffington Jr., 81-92, ASME, New York, 1965.

10. Sharpe, W.N., "Dynamic Strain Measurements with the Interferometric Strain Gage," Experimental Mech., 10(2), 89-92, 1970.

11. Karnes, C.H., "The Plate Impact Configuration for Determining Mechanical Properties of Materials at High Strain Rates," Mechanical Behavior of Material Under Dynamic Loads, ed. by U.S. Lindholm, 270-293, Springer-Verlag, Berlin, 1968.

12. Clifton, R.J., "Some Recent Developments in Plate Impact Experiments," Propagation of Shock Waves in Solids, ed. by E. Varley, 27-40, ASME, New York, 1976.

13. Hsu, J.C.C. and Clifton, R.J., "Plastic Waves in a Rate Sensitive Material I. Waves of Uniaxial Stress," J. Mech. Phys. Solids, 22, 233-253, 1974.

14. Lindholm, U.S., "Some Experiments with the Split Hopkinson Pressure Bar," J. Mech. Phys. Solids, 12, 317-335, 1964.

15. Lindholm, U.S. and Yeakley, L.M., "High Strain-Rate Testing: Tension and Compression," Exp. Mech., 8, 1-9, 1968.

16. Davies, E.D.H. and Hunter, S.C., "The Dynamic Compression Testing of Solids by the Method of the Split Hopkinson Pressure Bar," J. Mech. Phys. Solids, 11, 155-179, 1963.

17. Baker, W.E. and Yew, C.H., "Strain-Rate Effects in the Propagation of Torsional Plastic Waves," J. Appl. Mech., 33, 917-923, 1966.

18. Duffy, J., Campbell, J.D. and Hawley, R.H., "On the Use of a Torsional Split Hopkinson Bar to Study Rate Effects in 1100-0 Aluminum," J. Appl. Mech., 38, 83-91, 1971.

19. Walsh, J.M., Rice, M.H., McQueen, R.G. and Yarfer, F.L., "Shock-Wave Compression of Twenty-Seven Metals. Equation of State of Metals," Phys, Rev., 108, 196-216, 1957.

20. Jahsman, W.E., "The Kolsky Apparatus for the Measurement of Dynamic Material Properties," Univ. of Colorado, Boulder, Rept. CUMER-68-3, July 1968.

21. Bhushan, B., "Experimental and Numerical Studies of Rate-Dependent Materials," Ph.D. Thesis, Univ. of Colorado, Boulder, April 1976.

22. Holt, D.L., Babcock, S.G., Green, S.J. and Maiden, C.J., "The Strain-Rate Dependence of Flow Stress in Some Aluminum Alloys," Trans. ASME, 60, 152-159, 1967.

23. Nicholas, T., "Strain-Rate and Strain-Rate-History Effects in Several Metals in Torsion," Exp. Mech., 11, 370-374, 1971.

24. Karnes, C.H. and Ripperger, E.A., "Strain Rate Effects in Cold Worked High-Purity Aluminum," J. Mech. Phys. Solids, 14, 75-88, 1966.

25. Samanta, S.K., "Dynamic Deformation of Aluminum and Copper at Elevated Temperatures," J. Mech. Phys. Solids, 19, 117-135, 1971.

26. Kishida, K. and Senda, K., "New Experimental Method for Determining Dynamic Stress-Strain Relation of Metals," Exp. Mech., 8, 567-571, 1968.

27. Nicholas, T., and Lawson, J.E., "On the Determination of the Mechanical Properties of Materials of High Strain Rates", J. Mech. Phys. Solids, 20, 57-64, 1972.

28. Dharan, C.K.H. and Hauser, F.E., "Determination of Stress-Strain Characteristics at Very High Strain Rates", Exp. Mech., 10, 370-376, 1970.

29. Hoggatt, C.R. and Recht, R.F., "Stress-Strain Data Obtained at High Rates Using an Expanding Ring," Exp. Mech., 9, 441-448, 1969.

30. Hoge, K.G., "Influence of Strain Rate on Mechanical Properties of 6061-T6 Aluminum Under Unaxial and biaxial States of Stress," Exp. Mech., 6, 204-211, 1966.

31. Bhushan, B. and Jahsman, W.E., "Measurement of Dynamic Material Behavior Under Nearly Uniaxial Strain Conditions," Int. J. Solids Structures, 14, 739-753, 1978.

32. Conn, A.F., "On the Use of Thin Wafers to Study Dynamic Properties of Metals," J. Mech. Phys. Solids, 13, 311-327, 1965.

33. Bell, J.F., "An Experimental Diffraction Grating Study of the Quasi-Static Hypothesis of the Split Hopkinson Bar Experiment," J. Mech., Phys. Solids, 14, 309-327, 1966.

34. Jahsman, W.E., "Reexamination of the Kolsky Technique for Measuring Dynamic Material Behavior," J. Appl. Mech., 38, 75-82, 1971.

35. Bertholf, L.D. and Karnes, C.H., "Two-Dimensional Analysis of the Split Hopkinson Pressure Bar System," J. Mech. Phys. Solids, 23, 1-19, 1975.

36. Nichoals, T., "An Analysis of the Split Hopkinson Bar Technique for Strain-Rate-Dependent Material Behavior," J. Appl. Mech., 40, 277-282, 1973.

37. Bell J.F., "On the Direct Measurement of Very Large Strain at High Strain Rates," Exp. Mech., 7, 1-7, 1967.

38. Bell, J.F., "The Dynamic Plasticity of Metals at High Strain Rates: An Experimental Generalization," Proc. of Behavior of Materials Under Dynamic Loading, 19-41, ASME, New York, 1965.

39. Khan, A.S., "Behavior of Aluminum During the Passage of Large Amplitude Plastic Waves," Int. J. of Mech. Sci., 15, 503-516, 1973.

40. Sharpe, W.N., "Dynamic Plastic Response of Foil Gages," Exp. Mech., 10(10), 408-412, 1970.

41. Barrowman, E.M., "High-elongation Strain Measurement," Exp. Tech., 7(10), 29-32, 1983.

42. Taylor, G.I., "The Plastic Wave in a Wire Extended by an Impact Load," Civil Defense Research Committee Report R.C. 329, British Ministry of Home Security, 1942.

43. von Karman, T., "On the Propagation of Plastic Deformation in Solids," National Defense Research Council Report A-29, OSRD 365, USA, 1942.

44. White, M.P. and Griffis, Le Van, "The Permanent Strain in a Uniform Bar due to Longitudinal Impact," National Defense Research Council Report A-71, OSRD 742, USA, 1942.

45. Bell, J.F., "The Physics of Large Deformation of Crystalline Solids," Springer-Verlag, New York, 1968.

46. Moon, H., "An Experimental Study of the Outer Yield Surface for Annealed Polycrystalline Aluminum," Acta Mechanica, 24, 191-208, 1976.

47. Bell, J.F., "A Physical Basis for Continuum Theories of Finite Strain Plasticity: Part I," Archive for Rational Mech. and Anal., 70, 319-338, 1979. Part II , Archive for Rational Mech. and Anal., 75, 103-126, 1981.

48. Bell, J.F., "On the Dynamic Elastic Limit," Exp. Mech., 22(7), 270-276, 1982.